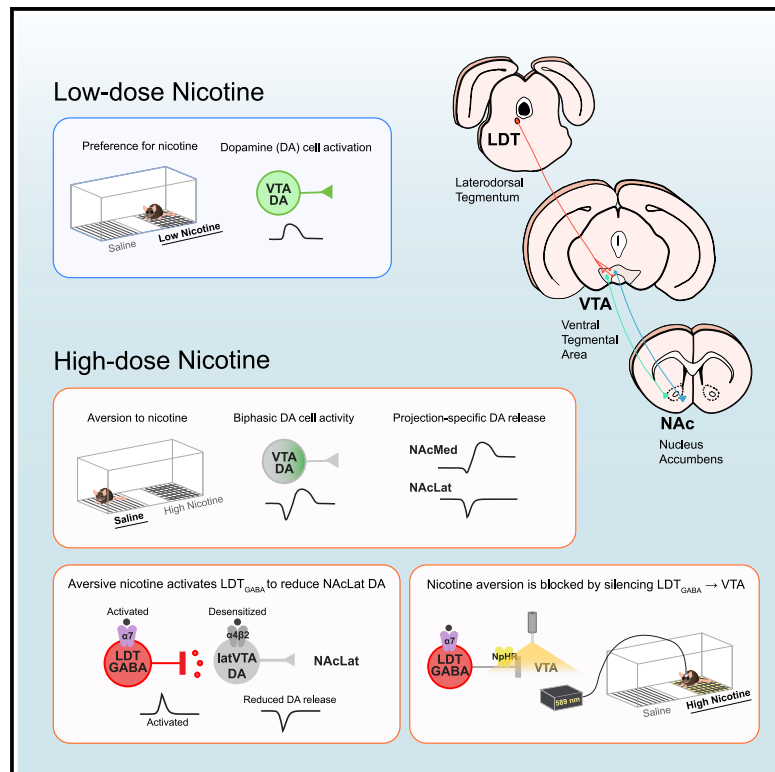


# An inhibitory brainstem input to dopamine neurons encodes nicotine aversion

## Graphical abstract



## Authors

Christine Liu, Amanda J. Tose,  
Jeroen P.H. Verharen, ..., Jessica X. Du,  
Kevin T. Beier, Stephan Lammel

## Correspondence

lammel@berkeley.edu

## In brief

Liu, Tose et al. reveal that a high dose of nicotine causes behavioral aversion and reduces dopamine release in the lateral nucleus accumbens through  $\alpha 7$  nicotinic acetylcholine receptors on an inhibitory brainstem input. Suppressing this input to dopamine neurons prevents the reduction of dopamine release and behavioral aversion to nicotine.

## Highlights

- Aversive nicotine promotes different DA release patterns in separate NAc subregions
- Modeling of  $\alpha 4\beta 2$  and  $\alpha 7$  nAChRs captures nicotine's dose-dependent effects
- Aversive nicotine reduces DA release in the lateral NAc through  $\alpha 7$  receptors
- LDT GABA cells mediate the effects of aversive nicotine on DA release and behavior

## Article

# An inhibitory brainstem input to dopamine neurons encodes nicotine aversion

Christine Liu,<sup>1,4</sup> Amanda J. Tose,<sup>1,4</sup> Jeroen P.H. Verharen,<sup>1</sup> Yichen Zhu,<sup>1</sup> Lilly W. Tang,<sup>1</sup> Johannes W. de Jong,<sup>1</sup> Jessica X. Du,<sup>1,3</sup> Kevin T. Beier,<sup>2</sup> and Stephan Lammel<sup>1,5,\*</sup>

<sup>1</sup>Department of Molecular and Cell Biology and Helen Wills Neuroscience Institute, University of California, California, Berkeley, CA 94720, USA

<sup>2</sup>Department of Physiology and Biophysics, University of California Irvine, 825 Health Sciences Road, Med Sci D320, Irvine, CA 92697, USA

<sup>3</sup>Present address: Neurobiology Section, Division of Biological Sciences, University of California, San Diego, La Jolla, CA 92037, USA

<sup>4</sup>These authors contributed equally

<sup>5</sup>Lead contact

\*Correspondence: [lammel@berkeley.edu](mailto:lammel@berkeley.edu)

<https://doi.org/10.1016/j.neuron.2022.07.003>

## SUMMARY

Nicotine stimulates the dopamine (DA) system, which is essential for its rewarding effect. Nicotine is also aversive at high doses; yet, our knowledge about nicotine's dose-dependent effects on DA circuits remains limited. Here, we demonstrate that high doses of nicotine, which induce aversion-related behavior in mice, cause biphasic inhibitory and excitatory responses in VTA DA neurons that can be dissociated by distinct projections to lateral and medial nucleus accumbens subregions, respectively. Guided by computational modeling, we performed a pharmacological investigation to establish that inhibitory effects of aversive nicotine involve desensitization of  $\alpha 4\beta 2$  and activation of  $\alpha 7$  nicotinic acetylcholine receptors. We identify  $\alpha 7$ -dependent activation of upstream GABA neurons in the laterodorsal tegmentum (LDT) as a key regulator of heterogeneous DA release following aversive nicotine. Finally, inhibition of LDT GABA terminals in VTA prevents nicotine aversion. Together, our findings provide a mechanistic circuit-level understanding of nicotine's dose-dependent effects on reward and aversion.

## INTRODUCTION

A predominant hypothesis for nicotine addiction is that nicotine "hijacks" natural reward processes in the brain (Dani and Harris, 2005; Laviolette and van der Kooy, 2004; Lüscher and Malenka, 2011; Picciotto and Kenny, 2021). However, nicotine's behavioral responses are dose dependent; nicotine is rewarding at low doses and acutely aversive at high doses (Fowler and Kenny, 2014; Fudala and Iwamoto, 1987; Fudala et al., 1985; Risinger and Oakes, 1995). Humans and animals maintain optimal blood nicotine levels by increasing consumption when nicotine levels are low and decreasing consumption when levels are too high (Ashton et al., 1979; Fowler and Kenny, 2011; St Helen et al., 2016). Notably, non-human primates will press a lever to stop additional infusions of nicotine (Goldberg et al., 1983). Although dose titration is common to other drugs of abuse like methamphetamine (Sambo et al., 2017), cocaine (Hnasko et al., 2007), and heroin (Loney et al., 2021), nicotine displays acutely aversive properties at high doses (Natarajan et al., 2011). While cocaine, methamphetamine, and ethanol can all generate an aversive phenotype in the conditioned place preference (CPP) task, this

effect is caused by delaying drug delivery until after animals have spent time in the conditioned chamber. When delivered before the conditioning period, the same doses of cocaine, methamphetamine, and ethanol induce CPP (Cunningham and Henderson, 2000; Ettenberg et al., 1999; Fudala and Iwamoto, 1990). To our knowledge, nicotine is the only drug observed to elicit an aversive phenotype in rodents both when the drug is delivered immediately before or after the conditioning period, suggesting its unique, acutely aversive effects (Fudala and Iwamoto, 1987). Nicotine's acutely aversive properties may explain the relative rarity of overdose compared with alcohol, heroin, and cocaine (Lachenmeier and Rehm, 2015). Furthermore, the aversive effects of nicotine can be experienced concurrently with the pleasurable effects (Sartor et al., 2010) and tolerance to high doses develops over time (Heishman and Henningfield, 2000), suggesting that nicotine aversion may be distinct from nicotine reward and tolerance to aversion may underlie the development of habitual nicotine consumption.

Recent research has pointed to a critical role of the habenulo-interpeduncular axis and its projections to the brainstem laterodorsal tegmentum (LDT) underlying the aversive actions of

nicotine (Antolin-Fontes et al., 2015; Fowler et al., 2011; Frahm et al., 2011; Hsu et al., 2013; Tuesta et al., 2017; Wolfman et al., 2018). In contrast, the rewarding and reinforcing effects of nicotine and other drugs of abuse involve dopamine (DA) neurons in the ventral tegmental area (VTA) that release DA in the nucleus accumbens (NAc) (Di Chiara and Imperato, 1988; Lüscher and Malenka, 2011). However, VTA<sub>DA</sub> neurons are not a monolith; subpopulations defined by anatomical location and projection target possess distinct properties and serve different functions (Brischoux et al., 2009; Lammel et al., 2012). The canonical reward prediction error encoding DA neurons are located in the lateral VTA (lVTA) and send projections to the lateral shell of the NAc (NAcLat), while medial VTA<sub>DA</sub> neurons send projections to the ventro-medial shell of the NAc (NAcMed) and release DA in response to aversive stimuli and cues that predict them (de Jong et al., 2019). Whether distinct DA subcircuits that regulate reward and aversion underlie nicotine's dose-dependent effects remains uncertain.

Nicotine's effects on DA neurons are exerted through nicotinic acetylcholine receptors (nAChRs) (Graupner et al., 2013; Klink et al., 2001; Tapper et al., 2004). Experimental and modeling studies suggest that the activation of  $\beta 2$ -containing nAChRs ( $\beta 2^*Rs$ ) and  $\alpha 7$ -containing nAChRs ( $\alpha 7Rs$ ) mediate nicotine self-administration, with  $\beta 2^*Rs$  primarily expressed directly on VTA<sub>DA</sub> cells to increase firing rate and  $\alpha 7Rs$  on excitatory inputs that are responsible for burst firing and synaptic plasticity (Besson et al., 2012; Gao et al., 2010; Mameli-Engvall et al., 2006; Mansvelder and McGehee, 2000; Mansvelder et al., 2002; Markou and Paterson, 2001; Picciotto et al., 1998; Schilström et al., 2003). However, nicotine also desensitizes nAChRs, rendering them temporarily inactive, thus preventing further activation by endogenous acetylcholine or nicotine (Fenster et al., 1997; Picciotto et al., 2008; Wooltorton et al., 2003). Importantly, disruption of VTA  $\alpha 7Rs$  and  $\beta 2^*Rs$  can alter aversive and reward-related behavior in response to intra-VTA infusions of low concentrations of nicotine (Laviolette and van der Kooy, 2003). However, much of the work characterizing nAChRs and nicotine-related behaviors focused on lower doses that are reinforcing, therefore less is known about how high, aversive doses of systemic nicotine act on nAChRs to modulate DA cell activity and release.

## RESULTS

### A computational model predicts divergent effects of rewarding versus aversive nicotine on dopamine cell activity

In animal experiments, nicotine is often delivered via intraperitoneal (i.p.) or subcutaneous (s.c.) injections (Fudala and Iwamoto, 1987; Saal et al., 2003). However, the needle-poke from an injection is an aversive stimulus that may obscure the acute, aversive effects of nicotine on DA release. We therefore developed an intravenous (i.v.) infusion protocol that reliably induced dose-dependent CPP or conditioned place aversion (CPA) in response to infusions of low and high doses of nicotine, respectively. On day 1, mice freely explored the behavior box for 10 min to obtain a pre-test baseline preference score for either chamber. On days 2–4, each mouse received saline in the morning while confined to

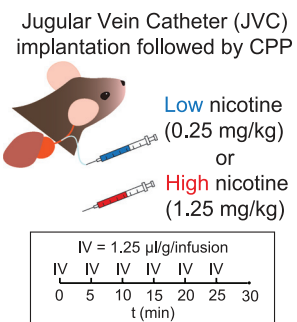
one chamber and nicotine in the afternoon while confined to the opposite chamber. Mice were randomly assigned to receive low or high nicotine doses. Infusions were delivered every 5 min through an implanted jugular vein catheter (JVC), for a total of 6 infusions over 30 min (Figures 1A–1D). The 5-min interval between infusions allows the accumulation of nicotine to observe neural activity dynamics as brain nicotine concentration increases over time (Taylor et al., 2013; Tolu et al., 2013). On day 5, animals again freely explored the behavior box for 10 min to obtain a post-test preference score. By assessing time spent in each chamber during the post-test compared with the pre-test, we found that mice receiving the low dose of nicotine spent more time in the nicotine-paired chamber indicating a preference, whereas mice receiving the high dose spent less time in the nicotine-paired chamber indicating aversion.

To predict VTA<sub>DA</sub> neuron activity in response to our i.v. nicotine protocol, we computationally modeled cell activation as a function of nicotine's effects on nAChRs containing  $\alpha 4$  and  $\beta 2$  subunits ( $\alpha 4\beta 2Rs$ ), which are highly expressed on VTA<sub>DA</sub> neurons and mediate nicotine's effects on DA release and behavioral reinforcement through direct activation and desensitization (Picciotto et al., 2008). For our model, we leveraged parameters established by Graupner, Maex, and Gutkin, who demonstrated a mechanism for nicotine-induced VTA<sub>DA</sub> cell inhibition via  $\alpha 4\beta 2R$  desensitization, disrupting activation of the receptor by endogenous acetylcholine (Graupner et al., 2013). To adapt their acute nicotine model to our nicotine infusion protocol, we modeled blood nicotine concentration from 6 nicotine infusions 5 min apart based on the half-life of nicotine in mice (Matta et al., 2007; Petersen et al., 1984). A single infusion of the aversive dose of nicotine is expected to activate and desensitize most of the  $\alpha 4\beta 2Rs$  immediately, leaving them in an inactive state for subsequent infusions (Figures 1E and 1F). Consequently, the modeled VTA<sub>DA</sub> cell response (expressing solely  $\alpha 4\beta 2Rs$ ) to the aversive dose of nicotine is a large increase in activity in response to the first infusion, whereas subsequent nicotine infusions decrease VTA<sub>DA</sub> activity relative to baseline (Figures 1G and 1H). Thus, VTA<sub>DA</sub> cells are predicted to be inhibited by aversive nicotine due to the disruption of baseline activation by endogenous acetylcholine after  $\alpha 4\beta 2Rs$  are desensitized. The rewarding dose, however, is modeled to desensitize  $\alpha 4\beta 2Rs$  at a gradual rate which maintains VTA<sub>DA</sub> cell activation, albeit with decreasing magnitude for each nicotine infusion. On average, the net effect of all nicotine infusions combined on VTA<sub>DA</sub> cell activity is expected to be greater in response to a rewarding dose of nicotine (Figure 1I), which is consistent with the role that increased and decreased rates of DA transmission is thought to have on promoting reward and aversion, respectively (Bromberg-Martin et al., 2010; Schultz, 1997; Tsai et al., 2009).

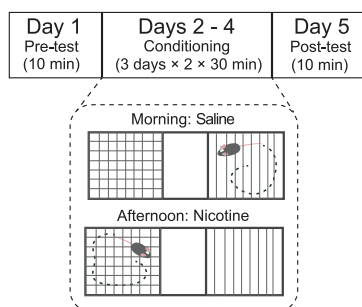
Could nicotine's actions solely through  $\alpha 4\beta 2Rs$  on VTA<sub>DA</sub> neurons mediate its dose-dependent behavioral effects? A computational model of our i.v. infusion protocol suggests that the rewarding dose of nicotine activates  $\alpha 4\beta 2Rs$  on VTA<sub>DA</sub> cells while the aversive dose desensitizes  $\alpha 4\beta 2Rs$ . Enhancing or disrupting the function of  $\alpha 4\beta 2Rs$  on VTA<sub>DA</sub> cells relative to baseline activity is modeled to give rise to dose-dependent VTA<sub>DA</sub> cell activation and inhibition, respectively. This model suggests that a high, aversive dose of nicotine can reduce VTA<sub>DA</sub> cell firing

Nicotine conditioned place preference (CPP) and aversion (CPA)

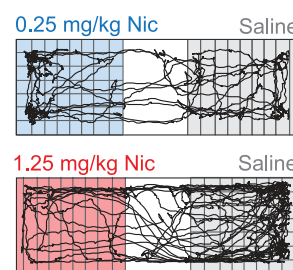
**A Experimental procedure**



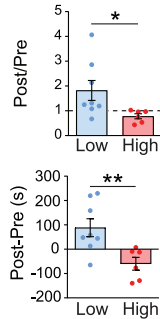
**B Conditioning protocol**



**C Sample post-test traces**



**D Preference scores**

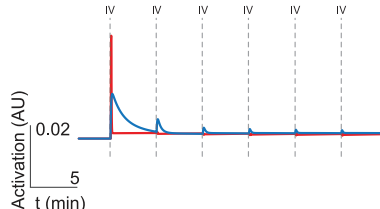


Computational model of VTA dopamine cell response to rewarding and aversive nicotine

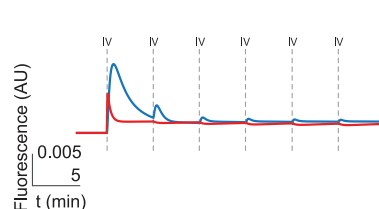
**E Modeled blood nicotine concentration**



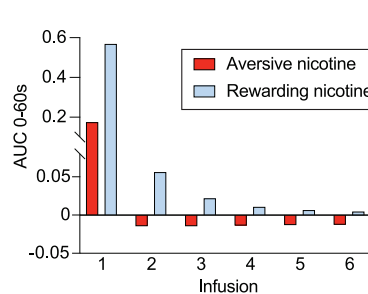
**F Modeled  $\alpha 4\beta 2$  receptor activation**



**G Modeled VTA DA GCaMP**



**H Modeled response to each infusion**



**I Modeled averaged GCaMP response**

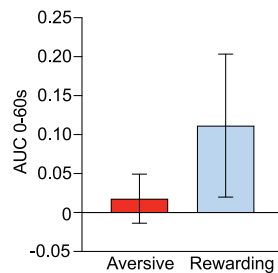


**Figure 1. Dose-dependent effects of nicotine on behavior and modeled VTA<sub>DA</sub> cell activity**

(A) Schematic of experimental design (CPP, conditioned place preference; CPA, conditioned place aversion).

(B) Timeline of experiment.

(C) Sample traces from representative animals during the post-test on day 5.

(D) Top: preference score as a ratio of time spent in the nicotine-paired chamber during the post-test relative to pre-test. Bottom: preference score as a difference between time spent in the nicotine-paired chamber during post-test relative to pre-test. (\*p < 0.05, \*\*p < 0.01; data represent means  $\pm$  SEM).

(E) Modeled blood nicotine concentration from aversive (red) and rewarding (blue) nicotine conditions during the 30-min infusion protocol.

(F) Modeled  $\alpha 4\beta 2$  receptor activation in response to aversive (red) and rewarding (blue) nicotine.

(G) Modeled GCaMP fluorescence in VTA<sub>DA</sub> neurons expressing  $\alpha 4\beta 2$  receptors in response to aversive (red) and rewarding (blue) nicotine.

(H) Modeled area under the curve (AUC) for 60 s post-infusion for each of 6 infusions during the 30-min infusion protocol.

(I) Modeled average AUC across all 6 infusions (data represent modeled means  $\pm$  SEM).

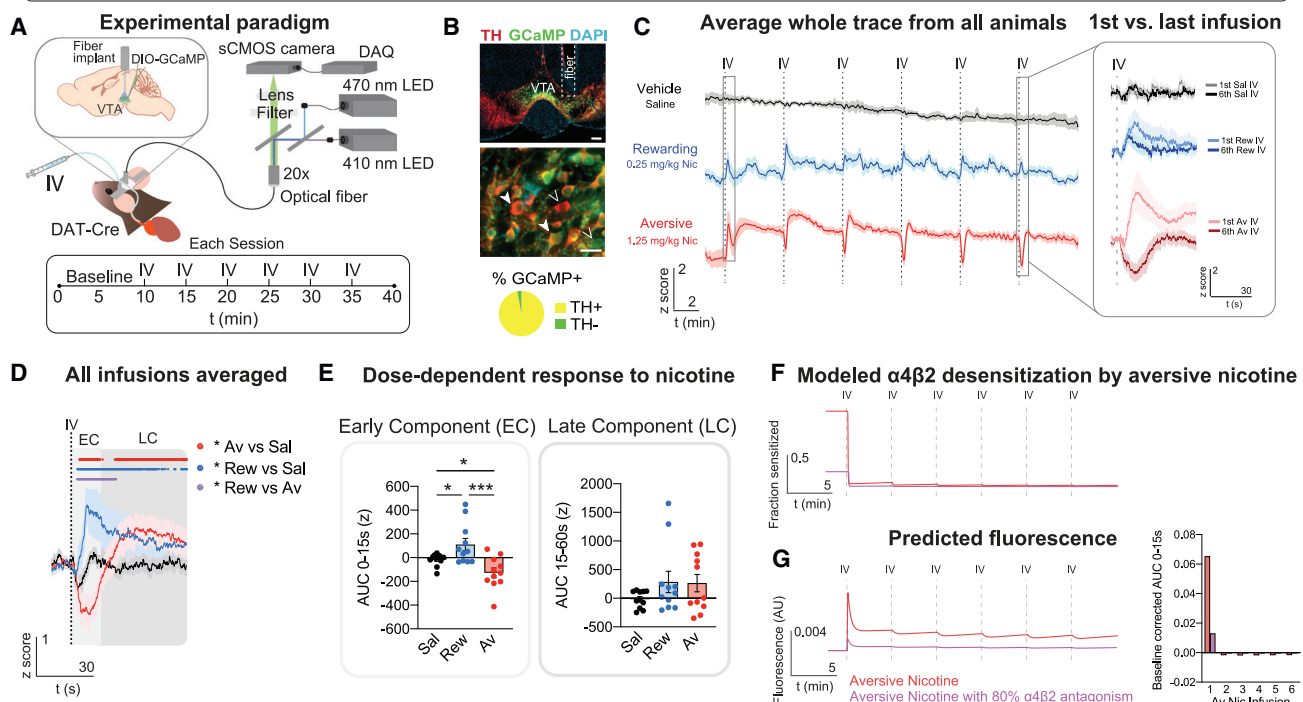
through  $\alpha 4\beta 2$ Rs, providing a quantitative hypothesis that can be tested experimentally.

**Aversive nicotine inhibits VTA dopamine cells when  $\alpha 4\beta 2$ Rs are desensitized**

To test the model predictions, we first examined the dose-dependent effects of nicotine on VTA<sub>DA</sub> neurons by performing

fiber photometry (FIP) experiments in awake, head-fixed animals. DAT-Cre mice were injected with an adeno-associated virus (AAV) carrying Cre-dependent GCaMP6m into the VTA, and an optical fiber was implanted to allow for the recording of calcium transients from VTA<sub>DA</sub> cell bodies in response to nicotine infusions. Calcium transients were recorded during the same 30-min i.v. protocol we established to induce nicotine preference

Fiber photometry recordings of VTA DA cells during IV infusions



VTA DA response to aversive nicotine with  $\alpha 4\beta 2$ R antagonism

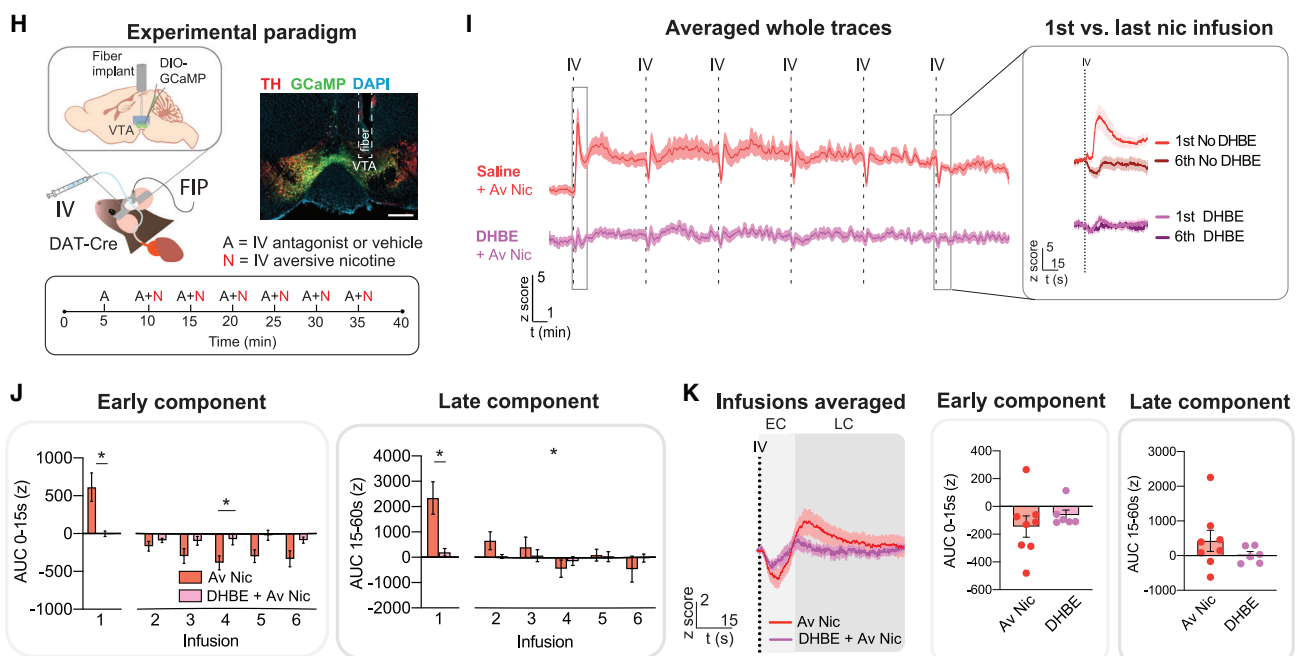


**Figure 2. Aversive nicotine suppresses VTA<sub>DA</sub> cell activity through  $\alpha 4\beta 2$  receptor desensitization**

(A) Top: schematic of a DAT-Cre mouse with AAV-DIO-GCaMP6m injected into VTA receiving i.v. infusions during fiber photometry recordings. Bottom: schematic showing timeline for i.v. nicotine or saline infusions.

(B) Top: optical fiber implant location in VTA (green, GCaMP; red, tyrosine hydroxylase [TH]; blue, DAPI; scale bars, 200  $\mu$ m). Middle: enlarged view (scale bars, 25  $\mu$ m). Bottom: 97% of GCaMP+ neurons are TH-immunopositive (yellow) and 3% are TH-immunonegative (green).

(legend continued on next page)

or aversion after an initial 10-min baseline acclimation period (Figures 2A, 2B, and S1A). We found that while saline infusions had minor, if any, effects on VTA<sub>DA</sub> activity, each infusion of the rewarding dose of nicotine consistently activated VTA<sub>DA</sub> cells (Figure 2C). As predicted by our computational model (Figure 1H), the first infusion of the high, aversive dose of nicotine activated VTA<sub>DA</sub> cells, and subsequent infusions suppressed cell activity (Figures 2C and S1E). However, our model did not predict such prominent inhibition, nor did it predict an activation of VTA<sub>DA</sub> cells beyond the first infusion that appears to wane with each infusion. By the final (i.e., sixth) infusion, VTA<sub>DA</sub> activity was strongly inhibited by nicotine (Figure 2C, inset). Because the complete series of nicotine infusions was necessary to promote CPP or aversion (Figures 1A–1D), we calculated the average response of VTA<sub>DA</sub> cell activity across infusions to reveal the net effect of rewarding or aversive nicotine. As a result, the rewarding dose of nicotine significantly activated VTA<sub>DA</sub> cells, whereas infusions of an aversive dose caused a biphasic response with an inhibitory early component (EC) lasting 15 s post-infusion and an excitatory late component (LC) from 15–60 s (Figures 2D, 2E, and S1D–S1F). Importantly, we counterbalanced the nicotine dose (rewarding or aversive) that animals received first to measure within-animal differences, and there was no order effect of nicotine doses (Figures S1B and S1C).

Our model of nicotine's effects on VTA<sub>DA</sub> cells through  $\alpha 4\beta 2$ Rs captured the general trend of activation by low, rewarding nicotine and desensitization after the first infusion of high, aversive nicotine. However, the biphasic response was not predicted; the inhibition during the 0–15 s EC was far greater in amplitude than expected, and the increase in activity during the 15–60 s LC was not predicted at all. Next, we followed up on the most salient prediction of the model, that  $\alpha 4\beta 2$ R desensitization explains the difference between the first and subsequent infusions, by generating a testable hypothesis for pharmacological antagonism of  $\alpha 4\beta 2$ Rs with our computational model. Mimicking receptor desensitization can be achieved by blocking receptor

activation with the competitive antagonist dihydro-beta-erythroidine (DHBE), which is selective for  $\beta 2$ -containing nAChRs (Rice and Cragg, 2004). Because DHBE can become non-specific or fatal at high doses (Damaj et al., 1999), we modeled an 80% blockade of  $\alpha 4\beta 2$ Rs to predict how DHBE treatment would affect VTA<sub>DA</sub> cell activity during infusions of aversive nicotine (Figures 2F and 2G). DHBE treatment is predicted to disrupt the effects of aversive nicotine predominantly on the first infusion because both DHBE and aversive nicotine should desensitize a majority of  $\alpha 4\beta 2$ Rs upon delivery, and infusions 2–6 of aversive nicotine are theorized to occur while  $\alpha 4\beta 2$ Rs are already desensitized. To test this prediction, we combined FIP of VTA<sub>DA</sub> cells with DHBE pharmacology. To ensure that DHBE could take effect before the introduction of nicotine and that its effects would persist for the entire duration of the infusion protocol, we pre-treated animals with i.v. DHBE 5 min into the initial baseline recording period, and then co-infused DHBE with aversive nicotine at the same dosage and intervals as in previous experiments (Figures 2H and S1G). Systemic delivery of antagonists is most comparable to systemic pharmaceutical treatment in humans, and co-infusion with nicotine allows constant availability of antagonists without additional stimuli mid-session; for example, a needle-poke or intrabrain infusion, preventing stimulus responses that may occlude the acute effects of nicotine infusion. Indeed, systemic DHBE reproduced the prediction from our computational model (Figure 2G); it reduced the response of VTA<sub>DA</sub> cell activity to aversive nicotine, significantly reducing activation from the first infusion with minor effects during infusions 2–6 (Figures 2I and 2J). The replication of our model prediction supports the hypothesis that  $\alpha 4\beta 2$ Rs play a role in activating VTA<sub>DA</sub> cells but become desensitized by a high dose of nicotine. The persistent, desensitized state of  $\alpha 4\beta 2$ Rs during nicotine exposure may be critical to the inhibition of VTA<sub>DA</sub> cells in response to aversive nicotine. However, the effects of DHBE on the biphasic response of VTA<sub>DA</sub> cells to aversive nicotine are inconclusive; the qualitative but not statistically significant

(C) Averaged GCaMP activity of VTA<sub>DA</sub> neurons in response to saline (gray), rewarding (blue), and aversive nicotine (red). Inset: overlays of averaged response to the first and sixth infusion for each condition. Light shading represents SEM.

(D) Averaged GCaMP activity of all six infusions showing 0–60 s post-infusion in response to saline (gray), rewarding (blue), and aversive nicotine (red) (data represent means  $\pm$  SEM). Dots above traces represent time points with significant differences between conditions from a multiple comparisons test (red, aversive nicotine versus saline; blue, rewarding nicotine versus saline; purple, rewarding versus aversive nicotine). Gray backgrounds distinguish the approximate time windows during which the response to aversive nicotine and saline are significantly different (i.e., light gray: 0–15 s [EC, early component]; dark gray: 15–60 s [LC, late component]) (\* $p < 0.05$ ; light shading represents SEM).

(E) Left: AUC for GCaMP response during EC (0–15 s) is significantly lower in the aversive nicotine (Av, red) condition compared with saline (Sal, black) and rewarding nicotine (Rew, blue). Right: no significant differences between conditions during the LC (15–60 s) (\* $p < 0.05$ , \*\* $p < 0.001$ ; data represent means  $\pm$  SEM).

(F) Computational modeling of  $\alpha 4\beta 2$ R desensitization by aversive nicotine predicts reduced sensitization in the presence of 80% antagonism of  $\alpha 4\beta 2$ Rs (purple) compared with that without  $\alpha 4\beta 2$ R antagonist (red).

(G) Left: predicted fluorescence in arbitrary units (AUs) based on computational modeling of  $\alpha 4\beta 2$ R activity as whole traces. Right: baseline-corrected AUCs during the EC (0–15 s) predict reduced excitation in response to the first infusion and reduced inhibition during infusions 2–6.

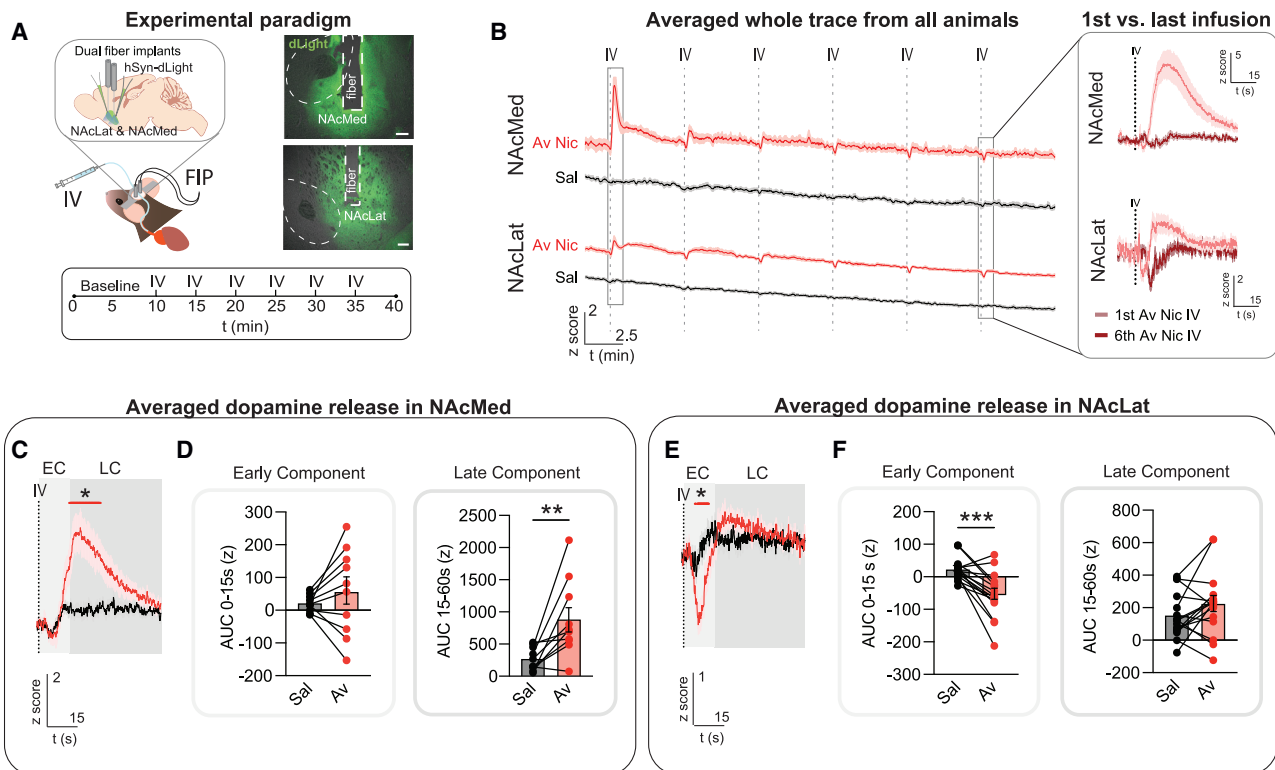
(H) Left and bottom: schematic showing AAV infusion and implantation of optical fibers in VTA of DAT-Cre mice. Fiber photometry recordings of VTA<sub>DA</sub> neurons are performed during infusions of aversive nicotine (red) with antagonist pre-treatment and co-infusion (gray). Right: anatomical verification of recording location in VTA (red, TH; green, GCaMP; blue, DAPI; scale bars, 500  $\mu$ m).

(I) Averaged whole traces of VTA<sub>DA</sub> GCaMP activity in response to aversive nicotine (Av Nic) without DHBE (red) and with DHBE (purple). Inset: comparison of response to the first and sixth infusions (area of light shading represents SEM).

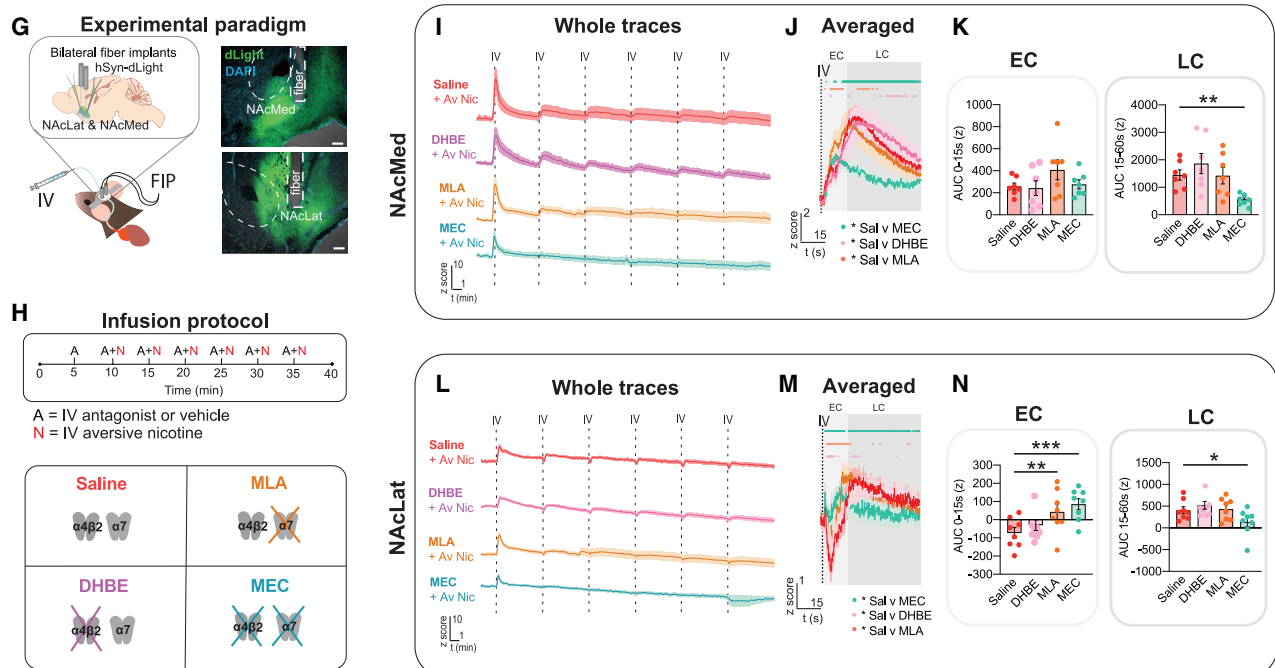
(J) Averaged AUCs for each infusion during the EC (0–15 s; left) and LC (15–60 s; right) (gap denotes separate analyses for infusion 1 and infusions 2–6 due to non-normal distribution, \* $p < 0.05$ , data represent means  $\pm$  SEM).

(K) Left: averaged traces of all 6 infusions showing 0–60 s post-infusion in response to aversive nicotine without DHBE (red) and in presence of DHBE (purple) (light shading represents SEM). Middle: averaged AUC response across infusions during the EC (data represent means  $\pm$  SEM). Right: averaged AUC response across infusions during the LC (data represent means  $\pm$  SEM).

Fiber photometry recordings of dLight response to aversive nicotine in NAc subregions



dLight recordings during aversive nicotine with nAChR antagonism



(legend on next page)

difference between averaged EC and LC responses do not explain the role of  $\alpha 4\beta 2$ Rs in mediating cell activity during either time component (Figure 2K). Further, the strength of inhibition in the EC and the observed increase in LC activity was not predicted by our model that assumed VTA<sub>DA</sub> neurons are a homogeneous population solely expressing  $\alpha 4\beta 2$ Rs. This shortcoming necessitates the investigation of other receptors or cell populations in mediating VTA<sub>DA</sub> population activity in response to nicotine.

### Aversive nicotine reduces dopamine release in the lateral mesoaccumbal pathway through $\alpha 7$ receptors

The biphasic inhibitory and excitatory responses to aversive nicotine may arise from heterogeneous VTA<sub>DA</sub> cell populations with different projection targets (de Jong et al., 2019; Verharen et al., 2020). To explore this possibility, we injected the DA sensor dLight1.2 into the NAcMed and NAcLat and implanted optical fibers to measure DA release in both regions simultaneously within animals. Each animal received i.v. infusions of saline and aversive nicotine on subsequent days while DA release was recorded (Figures 3A and S2A). Our results show that an inhibitory EC occurs in the NAcLat, whereas a significant increase of DA release can be observed during the LC in the NAcMed, confirming our hypothesis that the biphasic activity from the bulk VTA<sub>DA</sub> cell body signal could be dissociated by projection target (Figures 3B–3F). Notably, the increase of DA release in NAcMed occurs primarily in response to the first infusion of aversive nicotine before  $\alpha 4\beta 2$ Rs are desensitized, and the decrease of DA release in NAcLat occurs after  $\alpha 4\beta 2$ R desensitization by the first infusion (Figures S2E and S2F). In a separate experiment, we confirmed the behavioral relevance of reduced

DA release in NAcLat; optogenetic silencing of VTA<sub>DA</sub> terminals in NAcLat was sufficient to promote real-time place aversion, suggesting that inhibition of DA release in NAcLat is a crucial component of promoting aversion to high doses of nicotine (Figures S2H–S2J). We also recorded DA release in response to a rewarding dose of nicotine and found that there were no differences between NAcMed and NAcLat (Figures S2B and S2C), in accordance with previous research (Nguyen et al., 2021), nor was there an order effect of nicotine dose (Figure S2D). A comparison of dLight1.2 fluorescence and terminal GCaMP6m fluorescence in response to aversive nicotine showed no differences, further demonstrating the relationship between VTA<sub>DA</sub> cell activity and DA release in NAc subregions (Figure S2G).

Next, we sought to understand which nAChRs may mediate these divergent effects of aversive nicotine on DA release in NAc subregions. While our model of  $\alpha 4\beta 2$ R desensitization accurately predicted an inhibitory effect of aversive nicotine on VTA<sub>DA</sub> cells through disruption of activation by endogenous acetylcholine, we did not anticipate that a distinct subpopulation of DA neurons would be activated. A possible driver of this activation may be the recruitment of  $\alpha 7$ Rs, which require higher concentrations of nicotine to become activated and desensitized than  $\alpha 4\beta 2$ Rs (Fenster et al., 1997; Wooltorton et al., 2003). To explore how antagonism of  $\alpha 4\beta 2$  and  $\alpha 7$  receptors would alter DA release in the NAc, we carried out additional experiments in another cohort of animals with  $\alpha 4\beta 2$ R antagonist DHBE,  $\alpha 7$ R antagonist methyllycaconitine (MLA), and the non-specific nAChR antagonist mecamylamine (MEC) (Figures 3G–3N and S2K–S2M). We pre-treated animals with antagonist (or saline) 5 min into the initial baseline recording period then co-infused the antagonist with aversive nicotine at the same dosage and

**Figure 3. Aversive nicotine induces heterogeneous DA release patterns in distinct NAc subregions, which are modulated by nAChR antagonism**

(A) Left: schematic of simultaneous dLight fiber photometry (FIP) recordings in NAc medial shell (NAcMed) and NAc lateral shell (NAcLat) during i.v. infusions of saline or aversive nicotine. Right: dLight expression (green) and fiber implant location in NAcMed (top) and NAcLat (bottom). Dotted lines delineate NAc core (scale bars, 200  $\mu$ m). Bottom: schematic showing timeline for i.v. infusions.

(B) Averaged whole traces in response to aversive nicotine (Av Nic, red) and saline (Sal, black). Inset: comparison between first (light red) and sixth (dark red) infusions in the Av Nic condition (light shading represents SEM).

(C) Averaged response to all infusions for Av Nic (red) and Sal (black) in NAcMed. Dots above traces represent time points with significant differences (\* $p < 0.05$ ; light shading represents SEM).

(D) DA release in NAcMed significantly increased in response to Av Nic compared with Sal during the LC (right). No difference during the EC (left) (\*\* $p < 0.01$ ; data represent means  $\pm$  SEM).

(E) Averaged response to all infusions for Av Nic (red) and Sal (black) in NAcLat. Dots above traces represent time points with significant differences (\* $p < 0.05$ ; light shading represents SEM).

(F) DA release in NAcLat significantly decreased in response to Av Nic compared with Sal during the EC (left). No difference during the LC (right, dark gray border) (\*\* $p < 0.001$ ; data represent means  $\pm$  SEM).

(G) Left: schematic of simultaneous dLight FIP recordings in NAcMed and NAcLat during i.v. infusions of aversive nicotine with nAChR antagonists. Right: dLight (green) expression and optical fiber locations in the NAcMed (top) and NAcLat (bottom). Dashed lines delineate NAc core (blue, DAPI; scale bars, 200  $\mu$ m).

(H) Timeline and infusion protocol of aversive nicotine with nAChR antagonist pre-treatment and co-infusion of saline or nAChR antagonists ( $\alpha 7$  [MLA],  $\alpha 4\beta 2$  [DHBE] or non-specific [MEC]).

(I) Averaged whole traces of dLight in NAcMed in response to Av Nic with saline (red), DHBE (purple), MLA (orange), and MEC (turquoise) (light shading represents SEM).

(J) Averaged dLight response in NAcMed across all six infusions of Av Nic with saline (red), DHBE (purple), MLA (orange), and MEC (turquoise). Dots above traces represent time points with significant differences between each antagonist and the saline condition (\* $p < 0.05$ ; light shading represents SEM).

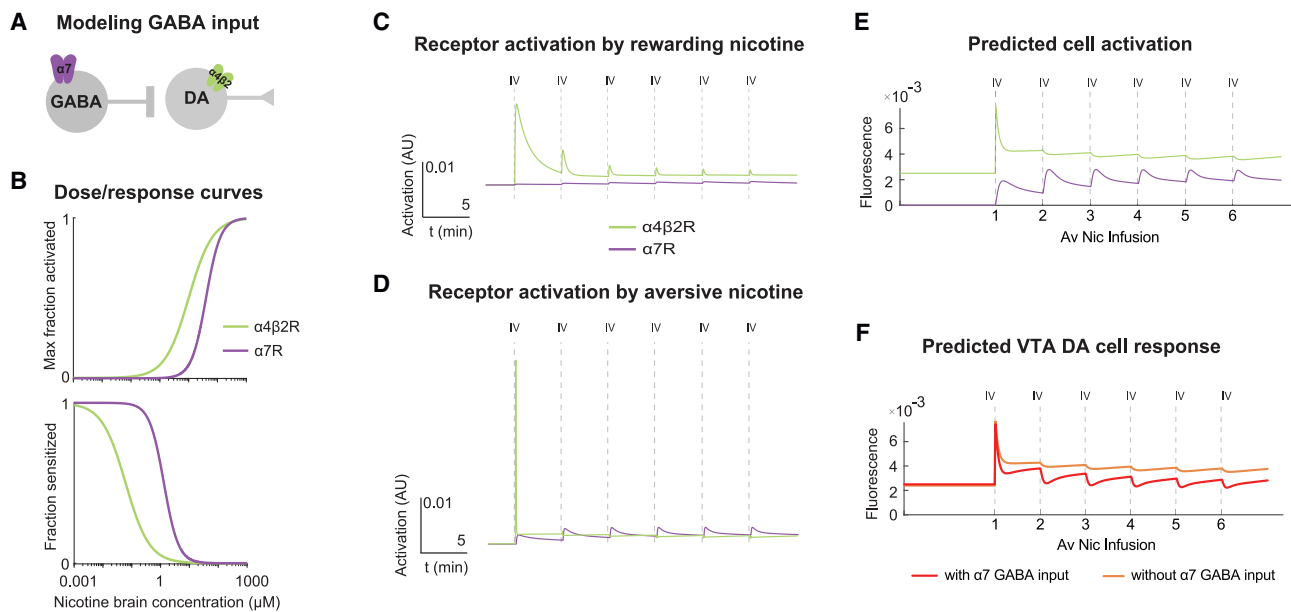
(K) Left: no significant differences in NAcMed dLight AUC during the EC. Right: during the LC, MEC significantly reduced NAcMed dLight AUC in response to Av Nic compared with no antagonist (saline) (\*\* $p < 0.01$ ; data represent means  $\pm$  SEM).

(L) Same as in (I), but for NAcLat.

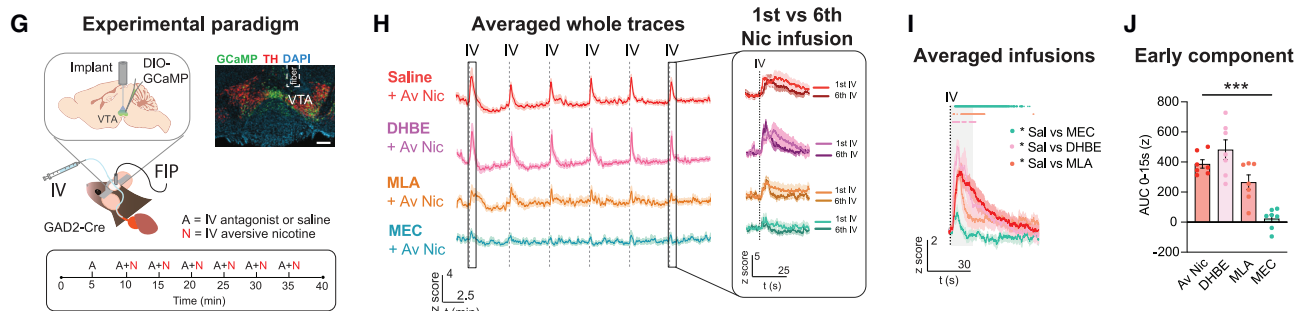
(M) Same as in (J) but for NAcLat.

(N) Left: during the EC, MLA, and MEC significantly attenuated the reduction of NAcLat dLight AUC to Av Nic. Right: during the LC, only MEC significantly reduced the NAcLat response to Av Nic (\* $p < 0.05$ , \*\* $p < 0.01$ , \*\*\* $p < 0.001$ ; data represent means  $\pm$  SEM).

Modeling contribution of  $\alpha 7$ -mediated inhibitory input to VTA DA neurons



Fiber photometry recordings of VTA GABA neurons



Fiber photometry recordings of LDT GABA terminals in VTA

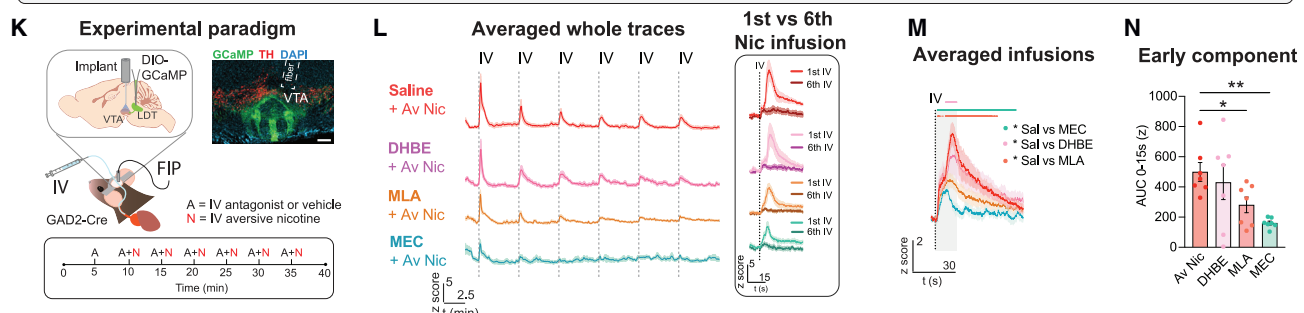


**Figure 4. Modeling and FIP recordings suggest putative role for  $\alpha 7$  nAChR modulation of LDT inhibitory inputs to VTA<sub>DA</sub> neurons for aversive nicotine-induced changes in DA release**

(A) Schematic of receptor expression and connectivity for predicting VTA<sub>DA</sub> cell activity as a function of  $\alpha 4\beta 2R$  (green) activity with inhibitory input under control of  $\alpha 7$  (purple) nAChRs.

(B) Dose/response curves demonstrating that  $\alpha 4\beta 2Rs$  (green) are activated and desensitized by lower concentrations of nicotine than  $\alpha 7$  (purple) nAChRs.

(C) Modeling receptor activation by rewarding nicotine based on our infusion protocol (Figure 1) predicts higher activation of  $\alpha 4\beta 2R$  (green) compared with  $\alpha 7R$  (purple) for each infusion, albeit with gradual desensitization.

(legend continued on next page)

intervals as in previous experiments (Figure 3H). Consistent with our hypothesis that  $\alpha 4\beta 2$ Rs drive activation specifically in response to the first infusion, EC DA release by the first infusion in both NAc subregions was decreased by DHBE (see infusion #1 in Figures 3I, 3L, S2L, and S2M). The absence of an effect on DA release in NAcLat by DHBE in subsequent infusions and when averaged across infusions is consistent with our recordings from VTA<sub>DA</sub> cell bodies and the hypothesis that DHBE and aversive nicotine share a common function to desensitize  $\alpha 4\beta 2$ Rs (Figures 2K and 3N). Furthermore, we found that LC activation was significantly reduced by MEC in both NAc subregions, but not by any other antagonists (Figures 3J, 3K, 3M, 3N, S2L, and S2M). Thus, receptors other than  $\alpha 4\beta 2$ Rs and  $\alpha 7$ Rs are likely involved in increasing DA release in response to aversive nicotine during the LC. Lastly, both MEC and MLA prevented the behaviorally relevant decrease of EC DA release in the NAcLat by aversive nicotine, indicating that  $\alpha 7$ R-mediated inhibition was blocked (Figure 3N). Our former hypothesis that  $\alpha 7$ Rs contributed to the activation of VTA<sub>DA</sub> cells through excitatory inputs to increase DA release in NAcMed was based on the known expression of  $\alpha 7$ Rs on glutamatergic inputs to VTA (Mansvelder and McGehee, 2000; Mansvelder et al., 2002). The surprising finding that  $\alpha 7$ Rs are required for the inhibition of DA release during the EC by aversive nicotine suggests a role for  $\alpha 7$ R-mediated inhibitory input to VTA<sub>DA</sub> neurons in nicotine aversion. These results suggest that a simple model of nicotine's dose-dependent actions on  $\alpha 4\beta 2$ Rs on VTA<sub>DA</sub> neurons alone is insufficient to explain the suppression of NAcLat DA release by aversive nicotine.

#### LDT GABA inputs to VTA are excited by aversive nicotine through $\alpha 7$ receptors

While  $\alpha 4\beta 2$  and  $\alpha 7$  receptors have both been implicated in nicotine reward and reinforcement, they possess distinct profiles in pharmacodynamics and anatomical expression (Figure 4A). Compared with  $\alpha 4\beta 2$ Rs that are expressed on VTA<sub>DA</sub> cells,  $\alpha 7$ Rs require higher concentrations of nicotine to become activated and desensitized (Figure 4B; Wooltorton et al., 2003). Thus, rewarding and aversive nicotine are expected to differentially affect  $\alpha 4\beta 2$  and  $\alpha 7$  receptors and the cells that express them. A rewarding dose of nicotine is modeled to activate

$\alpha 4\beta 2$ Rs with little effect on  $\alpha 7$ Rs, whereas aversive nicotine is predicted to activate  $\alpha 7$ Rs with each infusion and rapidly desensitize the majority of  $\alpha 4\beta 2$ Rs in the first infusion, rendering the  $\alpha 4\beta 2$ Rs unable to become activated by subsequent infusions of nicotine (Figures 4C and 4D). Thus, aversive nicotine should strongly activate a cell expressing  $\alpha 4\beta 2$ Rs in the first infusion and cause inhibition relative to baseline during subsequent infusions while reliably activating cells expressing  $\alpha 7$ Rs (Figure 4E). Based on our finding that suppression of DA release in NAcLat during the EC is mediated by  $\alpha 7$ Rs, a logical hypothesis is the existence of an inhibitory input to VTA<sub>DA</sub> cells that is activated by aversive nicotine through  $\alpha 7$ Rs (Figure 4A). Indeed, a previous study demonstrated that the inhibition of VTA<sub>DA</sub> firing rate in response to high doses of nicotine was blocked by GABA receptor antagonists (Erhardt et al., 2002). In this updated model, the predicted net effect of aversive nicotine on a cell expressing  $\alpha 4\beta 2$ Rs and receiving inhibitory input from a cell under the control of  $\alpha 7$ Rs is a slight reduction of activation from the first infusion and a stronger inhibition in response to subsequent infusions (Figure 4F).

Local VTA<sub>GABA</sub> neurons are a major inhibitory regulator of VTA<sub>DA</sub> neurons and are involved in nicotine reinforcement (Grieder et al., 2019; Tolu et al., 2013). Thus, VTA GABA cells are a candidate for reducing NAcLat DA release during the EC in response to aversive nicotine. We performed FIP recordings from GAD2-Cre mice that were infused with an AAV carrying Cre-dependent GCaMP6m and implanted with an optical fiber in the VTA (Figure S3A). An aversive dose of nicotine, but not a rewarding dose, significantly activated VTA GABA neurons (Figures S3B–S3E). To determine which receptors contribute to the activation of local VTA GABA neurons by aversive nicotine, we performed recordings in the presence of nAChR antagonists (Figure 4G). VTA GABA neurons were excited by aversive nicotine during the EC, and only the non-specific antagonist MEC significantly reduced this activation (Figures 4H–4J, S3F, and S3G). Although there was a small, but not significant, reduction in response to aversive nicotine during MLA treatment,  $\alpha 7$ Rs are unlikely to be the primary mediator of aversive nicotine-induced activation of local VTA GABA neurons.

Next, we decided to explore a different source of  $\alpha 7$ R-mediated inhibitory input to VTA<sub>DA</sub> cells. The brainstem LDT is a major

(D) Modeling receptor activation by aversive nicotine predicts that the majority of  $\alpha 4\beta 2$ Rs (green) are activated by the first infusion and exhibit decreased activation from infusions 2–6 due to receptor desensitization. Conversely,  $\alpha 7$ Rs (purple) are activated by each infusion of aversive nicotine.

(E) Predicted GCaMP fluorescence from a given cell expressing either  $\alpha 4\beta 2$ Rs (green) or  $\alpha 7$ Rs (purple) in response to aversive nicotine.

(F) Modeled VTA<sub>DA</sub> GCaMP activity in response to aversive nicotine with  $\alpha 4\beta 2$ R expression and inhibitory input under control of  $\alpha 7$ Rs (red; as shown in schematic A) or without inhibitory input (orange).

(G) Top: schematic showing FIP recordings from GCaMP-expressing VTA neurons in GAD2-Cre mice and i.v. infusions of saline, nicotine, and/or nAChR antagonists. Bottom: schematic showing timeline for i.v. administration of aversive nicotine and nAChR antagonists or saline. Right: fiber implant in VTA with GCaMP (green) and TH (red) expression (blue, DAPI; scale bars, 200  $\mu$ m).

(H) Averaged whole traces of VTA<sub>GABA</sub> GCaMP activity in response to Av Nic with co-infusion of saline (red), DHBE (purple), MLA (orange), and MEC (turquoise). Inset: comparisons between first and sixth infusion for each condition (light shading represents SEM).

(I) Averaged VTA GABA GCaMP activity for all 6 infusions in response to Av Nic with co-infusion of saline (red), MLA (orange), MEC (turquoise), and DHBE (purple). Dots above traces represent time points with significant differences from the saline condition (\*p < 0.05; light shading represents SEM).

(J) MEC significantly reduced VTA<sub>GABA</sub> GCaMP activity in response to Av Nic during the EC (\*\*p < 0.001, data represent means  $\pm$  SEM).

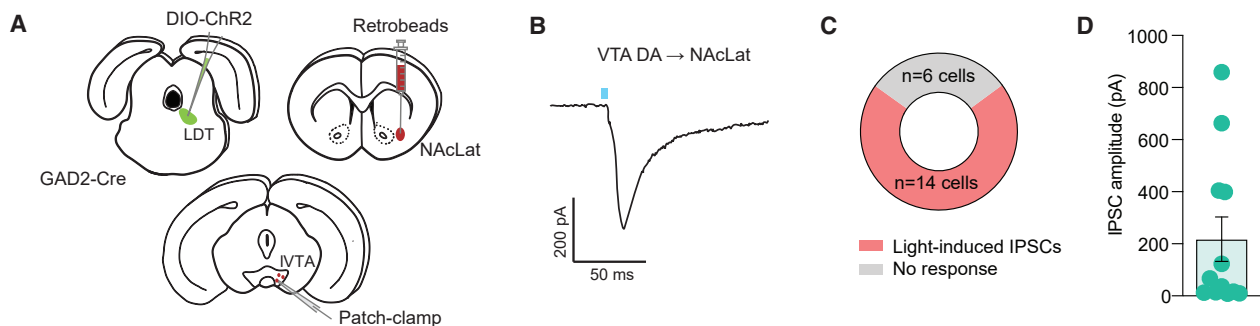
(K) Same experimental design as in (G), but for FIP recordings of LDT<sub>GABA</sub> terminals in the VTA.

(L) Same as in (H) but for LDT<sub>GABA</sub>  $\rightarrow$  VTA.

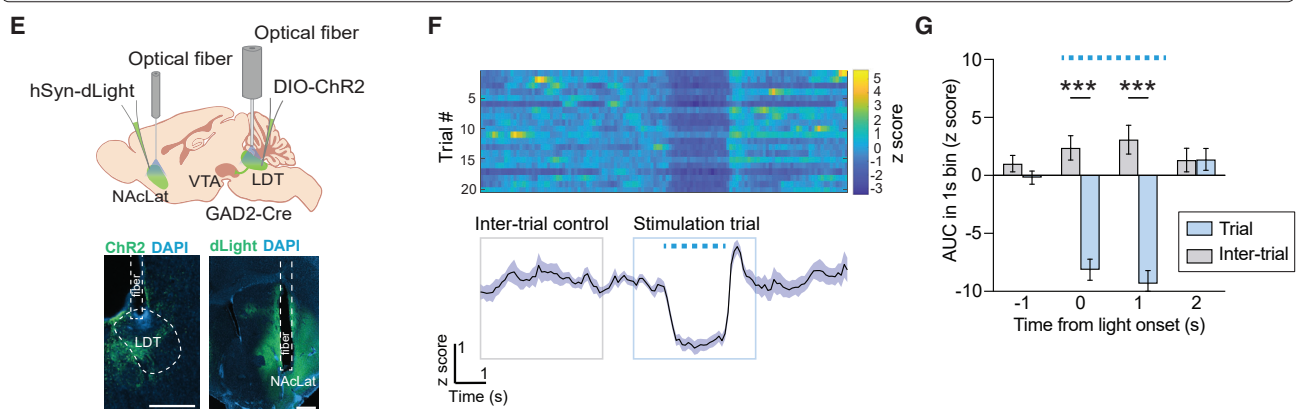
(M) Same as in (I) but for LDT<sub>GABA</sub>  $\rightarrow$  VTA.

(N)  $\alpha 7$  (MLA) and non-specific (MEC) nAChR antagonists reduced LDT<sub>GABA</sub>  $\rightarrow$  VTA activity response to Av Nic during the EC (\*p < 0.05, \*\*p < 0.01, data represent means  $\pm$  SEM).

*Ex vivo connectivity: LDT<sub>GAD2</sub> inputs to NAcLat-projecting VTA<sub>DA</sub> neurons*



*In vivo connectivity: Optogenetic stimulation of LDT<sub>GAD2</sub> neurons and dLight recordings in NAcLat*



*Behavior: Optogenetic stimulation of LDT<sub>GAD2</sub> terminals in VTA*

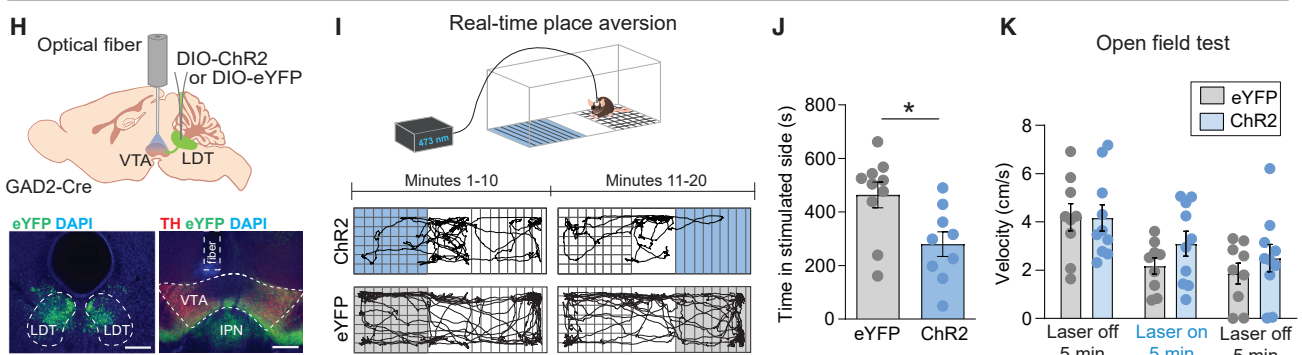


**Figure 5. Functional connectivity of LDT GABA neurons**

(A) GAD2-Cre animals ( $n = 8$  mice) were injected with AAV-DIO-ChR2 into LDT and fluorescent retrobeads into NAcLat. Patch-clamp recordings from retrogradely-labeled DA neurons in the lateral VTA (VTA).

(B) Representative light-induced IPSC from a bead-labeled VTA DA neuron.

(C) Proportions of recorded NAcLat-projecting DA cells that responded ( $n = 14$  cells, red) or did not respond ( $n = 6$  cells, gray) to light stimulation of LDT terminals in the VTA.

(D) Mean amplitude of light-induced IPSCs recorded from NAcLat-projecting DA cells ( $n = 14$  cells; data represent mean  $\pm$  SEM).

(E) Top: GAD2-Cre mice ( $n = 3$  mice) were injected with AAV-DIO-ChR2 into LDT, and an optical fiber was implanted above the LDT. The same mice received AAV-hSyn-dLight1.2 into NAcLat and an optical fiber was implanted into the NAcLat. Bottom: histological verification of ChR2 (green) expression and optical fiber location in the LDT (left) and dLight (green) expression and optical fiber location in the NAcLat (right) (blue, DAPI; scale bars, 500  $\mu$ m).

(F) Sample recording session with 20 trials. A 2 s pulse-train of 20 Hz 5 ms pulses of 3–5 mW 488 nm light was delivered to the LDT while dLight was simultaneously recorded in the NAcLat.

(G) Significant reduction in dLight signal during light stimulation when compared with dLight signal recorded between trials ( $^{***}p < 0.001$ , data represent mean  $\pm$  SEM).

(legend continued on next page)

excitatory input to VTA<sub>DA</sub> neurons, sending glutamatergic and cholinergic projections that mediate both natural reward and nicotine reward (Dautan et al., 2016; Kohlmeier, 2013; Lammel et al., 2012; Omelchenko and Sesack, 2005; Steidl et al., 2017). The LDT also contains a separate, non-overlapping population of GABAergic (i.e., GAD2-expressing, LDT<sub>GABA</sub>) neurons (Figure S4A; Soden et al., 2020; Wang and Morales, 2009), which comprise ~30% of LDT cells that project to the VTA (Figure S4B). LDT<sub>GABA</sub> neurons project more broadly to VTA and adjacent structures (e.g., interpeduncular nucleus [IPN]) compared to glutamatergic LDT (i.e., VGLUT2-expressing, LDT<sub>VGLUT2</sub>) neurons, which predominantly project to the IVTA (Figures S4C and S4D; Lammel et al., 2012). Although VTA-projecting LDT<sub>GABA</sub> neurons (LDT<sub>GABA</sub> → VTA) and VTA-projecting LDT<sub>VGLUT2</sub> (LDT<sub>VGLUT2</sub> → VTA) neurons receive qualitatively similar inputs, significant differences in the proportion of inputs were detected in the deep mesencephalic nucleus, dorsal raphe nucleus, parabrachial nucleus and locus coeruleus (Figures S4E–S4I). Using fluorescent *in situ* hybridization, we found that the majority of LDT neurons expressing  $\alpha 7R$  mRNA co-express GAD2 mRNA (Figures S4J and S4K). Importantly, brain-slice patch-clamp recordings revealed that LDT<sub>GABA</sub> neurons make direct inhibitory synaptic connections onto NAcLat-projecting VTA<sub>DA</sub> neurons (Figures 5A–5D) and *in vivo* optogenetic stimulation of LDT<sub>GABA</sub> neurons decreased DA release in the NAcLat (Figures 5E–5G) and promoted real-time place aversion (Figures 5H–5K) suggesting that LDT<sub>GABA</sub> neurons are another candidate for  $\alpha 7R$ -mediated inhibitory input to VTA<sub>DA</sub> neurons to encode nicotine aversion. Indeed, LDT<sub>GABA</sub> terminals in the VTA are selectively activated by aversive, but not rewarding, nicotine (Figures S5A–S5E). To test whether LDT<sub>GABA</sub> → VTA<sub>DA</sub> neurons could be the  $\alpha 7R$ -mediated source of inhibition, we performed FIP recordings from GAD2-Cre mice that have been infused with a 1:1 mix of AAV carrying Cre-dependent GCaMP6m and axon-targeted GCaMP6s into the LDT to improve fluorescent signal at axon terminals and implanted with an optical fiber in the VTA (Figure S5F). To determine which receptors contribute to the activation of LDT<sub>GABA</sub> → VTA neurons by aversive nicotine, we performed recordings with DHBE, MLA, and MEC treatment (Figure 4K). We found that both MEC and MLA reduce the EC activation in LDT<sub>GABA</sub> inputs to the VTA by aversive nicotine (Figures 4L–4N, S5G, and S5H).

Together, our results indicate that the activation of LDT<sub>GABA</sub> → VTA neurons by aversive nicotine is mediated by  $\alpha 7Rs$ , which makes this neural population a candidate for the inhibitory input in our model that drives the suppression of DA release in the NAcLat.

### Manipulation of LDT GABA cells alters the effects of aversive nicotine on dopamine release and behavior

To understand the role of  $\alpha 7R$ -mediated inhibitory inputs on VTA<sub>DA</sub> cells expressing  $\alpha 4\beta 2Rs$ , we updated our computational model and predicted that the absence of inhibitory inputs would cause slightly higher activation in response to the first infusion of aversive nicotine and less inhibition by subsequent infusions (Figures 6A–6C). To directly test the model prediction, we genetically ablated LDT<sub>GABA</sub> neurons and recorded DA release in response to aversive nicotine. Specifically, GAD2-Cre mice were injected in the LDT with an AAV carrying Cre-dependent mCherry (AAV-DIO-mCherry) as a control or a 1:1 mix of AAV-DIO-mCherry and AAV-flex-taCasp3 to induce apoptosis in infected neurons (Yang et al., 2013). dLight1.2 was injected into the NAcLat and NAcMed and optical fibers were implanted into these regions to allow simultaneous FIP recordings of DA release during i.v. infusions (Figures 6D, S6A, and S6B). Adequate ablation of LDT<sub>GABA</sub> cells by caspase was indicated by the absence of mCherry expression (Figures 6E, S6A, and S6B). In accordance with our model prediction, we found a significant attenuation of the EC DA reduction in the NAcLat and a reduction of the LC DA release in response to the first infusion (Figures 6F–6H and S6C). Surprisingly, animals injected with caspase in the LDT also showed a significant reduction in the LC of DA release in the NAcMed in response to aversive nicotine (Figures 6I–6K and S6D) indicating that LDT<sub>GABA</sub> neurons may directly and/or indirectly influence NAcMed-projecting DA neurons.

After establishing that ablation of LDT<sub>GABA</sub> neurons altered DA release in response to aversive nicotine, we sought to examine whether inhibition of the LDT<sub>GABA</sub> → VTA pathway affects the behavioral response to aversive nicotine. We bilaterally targeted the LDT of GAD2-Cre mice with an AAV carrying the Cre-dependent inhibitory opsin halorhodopsin (AAV-DIO-eNpHR) or eYFP (AAV-DIO-eYFP) as a control and implanted angled optic fibers bilaterally toward the VTA (Figure 6L). We found that control animals exhibited conditioned place aversion to high-dose nicotine, but nicotine aversion was not observed in the eNpHR group (Figures 6M–6P). Thus, inhibiting LDT<sub>GABA</sub> terminals in the VTA successfully blocked the aversive effects of a high dose of nicotine. Additionally, optogenetic inhibition of LDT<sub>GABA</sub> terminals in the VTA alone had no impact on behaviors unrelated to nicotine such as real-time place preference or open field locomotion (Figures S6E–S6G).

Collectively, these results establish that LDT<sub>GABA</sub> neurons (1) contribute to the heterogeneous patterns of DA release in distinct NAc subregions induced by aversive nicotine and (2) are necessary for nicotine-induced conditioned place aversion.

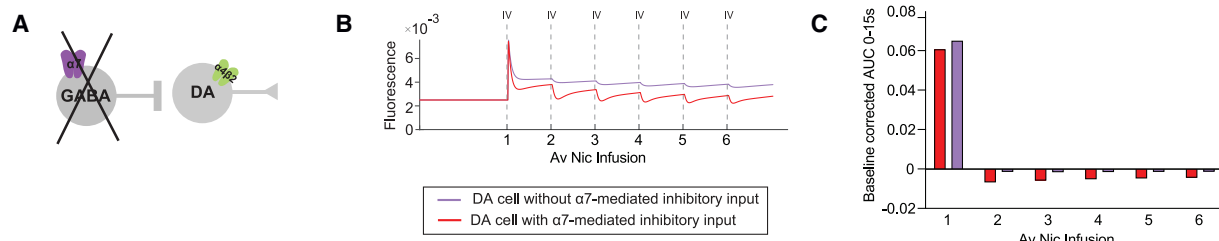
(H) Top: GAD2-Cre animals received bilateral injection of AAV-DIO-ChR2 (n = 9 mice) or AAV-DIO-eYFP (n = 10 mice) into LDT and an optical fiber was implanted above the VTA to optogenetically stimulate LDT<sub>GABA</sub> terminals in the VTA. Bottom: eYFP (green) expression in the LDT (left) and VTA (right). Note: optical fiber was placed above the VTA (blue, DAPI; red, TH; scale bars: 400  $\mu$ m [left] and 250  $\mu$ m [right]).

(I) Top: real-time place preference/avoidance paradigm. Bottom: movement of GAD2-Cre mice expressing ChR2 (top) or eYFP (bottom) in the LDT. Mice received 20-Hz light stimulation in the VTA when they entered the left (min 1–10) or right (min 11–20) side of the chamber.

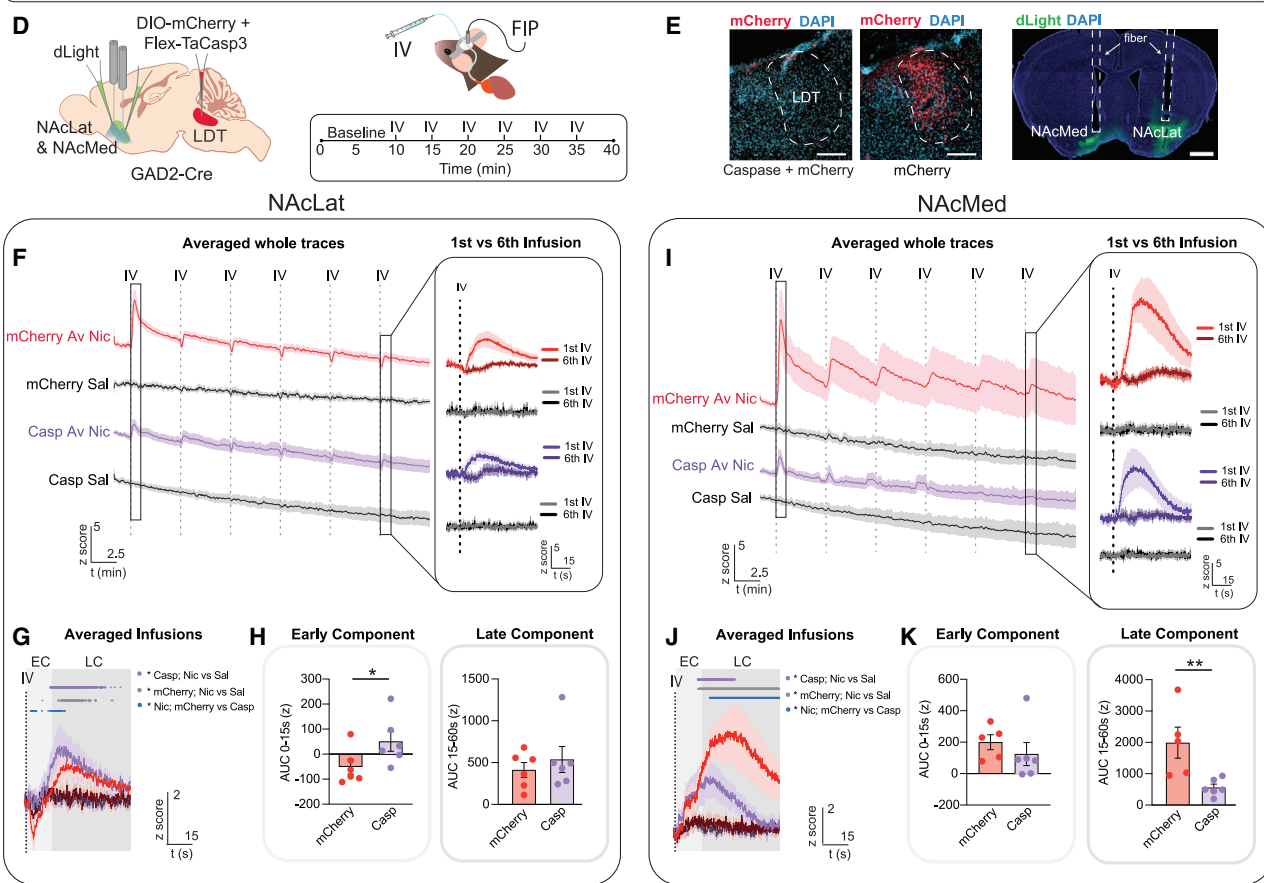
(J) Animals expressing ChR2 in the LDT spent significantly less time in the light-paired side of the chamber compared with eYFP-expressing mice (\*p < 0.05; data represent means  $\pm$  SEM).

(K) No significant difference in locomotor activity was observed in an open field test between ChR2- (blue, n = 9 mice) and eYFP-expressing (gray, n = 10 mice) GAD2-Cre mice before, during or after 20-Hz light stimulation (data represent means  $\pm$  SEM).

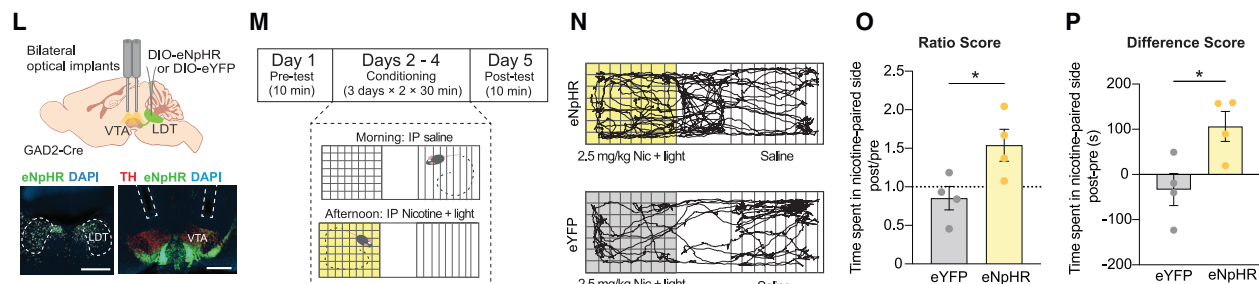
Modeling contribution of LDT GABA neurons in dopamine response to aversive nicotine



dLight recordings in NAc subregions after LDT GABA cell ablation



Optogenetic inhibition of LDT GABA terminals in VTA blocks the aversive effects of a high dose of nicotine



(legend on next page)

## DISCUSSION

### Effects of aversive nicotine in a heterogeneous dopamine system

Our study supports the view that the reward-enhancing and reward-inhibiting properties (i.e., anxiety) of low doses of nicotine recruit discrete, concurrent DA circuits (Nguyen et al., 2021), and establishes a novel mechanism for how high doses of nicotine alter DA signaling in separate mesoaccumbal DA subsystems. In line with previous work, we found that a rewarding dose of nicotine increased VTA<sub>DA</sub> activity (Imperato et al., 1986; Nguyen et al., 2021). However, a high, aversive dose of nicotine bidirectionally altered DA signaling by inhibiting a canonical reward pathway (NAcLat) and activating a distinct mesoaccumbal DA pathway (NAcMed) previously shown to be activated by aversive stimuli and cues that predict them (de Jong et al., 2019; Verharen et al., 2020). These results support the idea that NAc subregions have specialized roles in dissociating nicotine motivational signaling (Sellings et al., 2008). Future studies are needed to understand whether LDT<sub>GABA</sub> neurons directly or indirectly influence the medial mesoaccumbal DA pathway in response to aversive nicotine and whether other DA subsystems (e.g., mesoamygdaloid, mesoprefrontal) contribute to nicotine aversion.

### Bridging the habenulo-interpeduncular axis with the mesolimbic dopamine system

Previous studies have shown that the habenulo-interpeduncular axis (i.e., projections from the medial habenula [mHb] to IPN) is involved in fear, anxiety, nicotine withdrawal, and nicotine aversion (Antolin-Fontes et al., 2015; Fowler and Kenny, 2014). mHb

and IPN activity may signal the aversive effects of nicotine to downstream brain regions, such as the LDT (Wolfman et al., 2018). It is conceivable that a circuit mechanism for nicotine aversion may involve disinhibition of LDT<sub>GABA</sub> → VTA neurons to reduce DA release in the NAcLat. Such disinhibition could arise from inhibition of local LDT interneurons (Yang et al., 2016) through IPN neurons (Wolfman et al., 2018), which are directly excited by mHb cells (Fowler et al., 2011; Frahm et al., 2011). Future studies are needed to elucidate local connectivity within the LDT and simultaneous *in vivo* recordings of multiple brain regions in the habenulo-interpeduncular-mesopontine-axis may further reveal how a response to aversive nicotine is coordinated.

Because our ablation of LDT<sub>GABA</sub> cells targeted all GAD2-expressing LDT cells and terminal inhibition of LDT<sub>GABA</sub> → VTA neurons can affect collateral projections via back-propagating action potentials, we cannot exclude LDT<sub>GABA</sub> interneurons or those that project to regions other than the VTA in mediating the effects of aversive nicotine on DA release, including a direct inhibitory projection to the NAc (Coimbra et al., 2019). Although both nicotine and acetylcholine have the potential to directly and/or indirectly modulate striatal DA release (Cachope et al., 2012; Rice and Cragg, 2004; Threlfell et al., 2012), this mechanism seems unlikely in the case of LDT<sub>GABA</sub> → NAc neurons, given that optogenetic stimulation of LDT<sub>GABA</sub> → NAc inputs had no effect on place preference or aversion behavior (Coimbra et al., 2019), unlike the robust real-time place aversion we observed during LDT<sub>GABA</sub> → VTA stimulation. On the other hand, it is likely that LDT<sub>GABA</sub> neurons target additional cell populations beyond lateral VTA<sub>DA</sub> neurons given that ablation of neurons also reduced the LC DA release in the NAcMed in response

**Figure 6. Manipulation of LDT GABA neurons reduces the effects of aversive nicotine on DA release in the NAc and prevents nicotine-induced aversion**

(A) Schematic representation of modeling VTA<sub>DA</sub> cell activity with removal of  $\alpha$ 7R-mediated inhibitory inputs.

(B) Modeled GCaMP fluorescence of VTA<sub>DA</sub> neurons expressing  $\alpha$ 4 $\beta$ 2Rs with (red) and without (purple)  $\alpha$ 7R-mediated inhibitory input.

(C) Modeled baseline-corrected AUCs quantifying the EC of VTA<sub>DA</sub> GCaMP fluorescence in response to aversive nicotine without  $\alpha$ 7R-mediated inhibitory input (purple) predicts a slightly higher activation in response to the first infusion of aversive nicotine and decreased suppression in response to infusions 2–6.

(D) Schematic showing simultaneous FIP recordings of NAcMed and NAcLat dLight and i.v. infusions of aversive nicotine or saline in mice with genetic ablation of LDT GABA neurons.

(E) Left: histological verification of genetic ablation of LDT GABA neurons (Flex-TaCasp3, caspase group) compared with control animals (mCherry, red) (scale bars, 200  $\mu$ m). Right: optical fiber placement in NAcMed and NAcLat with dLight (green) expression (blue, DAPI; scale bars, 1 mm).

(F) Averaged whole-trace NAcLat dLight response to aversive nicotine Av Nic or saline in mice with genetic ablation of LDT GABA neurons or control animals (red, mCherry Av Nic; purple, caspase Av Nic; black—mCherry saline and caspase saline). Inset: comparisons of first and last infusions (light shading represents SEM).

(G) dLight response in NAcLat averaged across all 6 infusions of saline or Av Nic in mice with genetic ablation of LDT GABA neurons or control animals. Dots above the traces denote significant differences in a multiple comparisons test (purple, Av Nic versus saline in caspase group; gray, Av Nic versus saline in mCherry group; blue, Av Nic in mCherry versus caspase groups) (\* $p$  < 0.05; light shading represents SEM).

(H) Left: averaged NAcLat dLight AUC across infusions demonstrates more inhibition in mCherry mice compared with caspase mice in response to Av Nic during the EC. Right: no significant difference between groups during the LC (\* $p$  < 0.05, data represent means  $\pm$  SEM).

(I) Same as in (F) but for NAcMed.

(J) Same as in (G) but for NAcMed.

(K) Left: no significant difference between groups during the EC. Right: averaged NAcMed dLight AUC across infusions reveals significant reduction in Caspase AUC during the LC compared with mCherry (\* $p$  < 0.01, data represent means  $\pm$  SEM).

(L) Top: schematic showing AAV infusions of Cre-dependent halorhodopsin (DIO-eNpHR) or eYFP into LDT of GAD2-Cre mice with bilateral optical fibers above VTA. Bottom: eNpHR (green) expression in LDT neurons (left) and in LDT terminals in the VTA (right) with location of optical fiber implants (red, TH; blue, DAPI; scale bars, 500  $\mu$ m).

(M) Schematic of conditioned place aversion assay and timeline.

(N) Trajectories of sample eNpHR and eYFP mice during post-test (day 5). Yellow (and gray) indicates chamber side paired with light delivery.

(O) Preference score as a ratio of time spent in the nicotine-paired chamber during the post-test relative to pre-test. (\* $p$  < 0.05; data represent means  $\pm$  SEM).

(P) Preference score as a difference between time spent in the nicotine-paired chamber during post-test relative to pre-test. (\* $p$  < 0.05; data represent means  $\pm$  SEM).

to aversive nicotine, and terminals from  $LDT_{GABA}$  neurons were detected in the IPN.

Our work also reveals that  $VTA_{GABA}$  neurons are strongly activated by aversive nicotine. Previous work has shown that stimulation of  $VTA_{GABA}$  cell bodies produces conditioned place aversion (Tan et al., 2012) and that projection-specific  $VTA_{GABA} \rightarrow NAc$  stimulation impairs reward seeking (Lowes et al., 2021). Although our pharmacological experiments indicate that  $VTA_{GABA}$  neurons as a population are not strongly regulated by  $\alpha 7Rs$ , it remains unknown whether distinct subpopulations of  $VTA_{GABA}$  neurons could participate in the  $\alpha 7R$ -mediated suppression of NAcLat DA release by aversive nicotine.  $VTA_{GABA}$  neurons may therefore additionally contribute to nicotine aversion.

Despite the questions that remain regarding specific  $LDT_{GABA}$  and  $VTA_{GABA}$  neuronal subtypes in nicotine aversion, the neural circuit introduced here may explain how the habenulo-interpeduncular axis connects to the mesolimbic DA system via the brainstem mesopontine tegmentum.

### A computational model for nicotine's dose-dependent effects

The dose-dependent effects of nicotine on behavior are likely the culmination of responses by many nAChRs, brain regions, cell types, and other features that are difficult to integrate into one unifying theory. To avoid overcomplicating our model, we sought to fit as few parameters as possible that would account for the major dynamics observed to effectively simulate nicotine's dose-dependent effects on  $VTA_{DA}$  activity (Wilson and Collins, 2019). Further, isolating nicotine delivery to specific brain regions may have allowed a better understanding of each cell population's response, but systemic delivery is more relevant to human nicotine intake and pharmaceutical treatment.

Our methods balanced simplicity with specificity to model  $VTA_{DA}$  neurons as units under the control of direct receptor expression and the net effect of systemic nicotine on their inputs.

While rewarding nicotine activates  $\alpha 4\beta 2Rs$  and increases  $VTA_{DA}$  cell activity, an aversive dose desensitizes the receptors and  $VTA_{DA}$  cells are no longer activated by nicotine, rendering them more susceptible to inhibition from afferent inputs. Indeed, when we systemically antagonized  $\alpha 4\beta 2Rs$  with DHBE to mimic receptor desensitization,  $VTA_{DA}$  cell body activity was in alignment with our model.

The role of  $\alpha 7Rs$  in nicotine-related behaviors has been difficult to clarify, with contradictory findings about their role in nicotine reward, reinforcement, aversion, or lack thereof (Besson et al., 2012; Brunzell and McIntosh, 2012; Grottick et al., 2000; Laviolette and van der Kooy, 2003; Markou and Paterson, 2001). Nicotine CPP is blocked if  $\alpha 7R$  activity is enhanced during delivery of rewarding doses, by either pharmacological agonism or gain-of-function  $\alpha 7$  mutant mice (Harenza et al., 2014). Additionally, intra-brain infusion of an  $\alpha 7R$  agonist decreased motivation to work for nicotine, whereas infusion of an  $\alpha 7R$  antagonist increased motivation (Brunzell and McIntosh, 2012). Our results show that  $\alpha 7$  mRNA is expressed in  $LDT_{GABA}$  neurons, which are activated by a high, aversive dose of nicotine to inhibit  $VTA_{DA}$  neurons and decrease DA release in the NAcLat. Thus, nicotine's dual actions to recruit  $\alpha 7Rs$  and desensitize  $\alpha 4\beta 2Rs$  may

be important mechanisms in encoding nicotine reward and aversion.

The systemic, pharmacological antagonists used in our study can be non-specific at very high doses (Whiteaker et al., 2007). Therefore, cell-type-specific gene deletion strategies of nAChRs and more specific antagonists (Brunzell and McIntosh, 2012) could be used in future studies to further delineate their roles in nicotine reward and aversion.

### Relevance to treatments for nicotine addiction

Understanding the neurobiology of nicotine reward and aversion may inform the development of novel treatments to aid in nicotine cessation. Varenicline is currently the only available pharmaceutical designed specifically to support nicotine cessation. Prescribed to be taken daily, it partially agonizes  $\alpha 4\beta 2Rs$  to provide relief from nicotine withdrawal and reduces nicotine-induced DA release (Coe et al., 2005; McCaul et al., 2020). Indeed, a recent study demonstrated that both  $VTA_{DA}$  cell activity and DA release in NAcLat in response to i.p. nicotine was reduced by varenicline (Goldstein et al., 2022). Because varenicline is also a full agonist at  $\alpha 7Rs$  and the binding of varenicline to  $\alpha 4\beta 2Rs$  appears to favor the desensitized state (Mihalak et al., 2006), its effects may be explained by increasing nicotine aversion and decreasing nicotine reward through the mechanisms characterized in our study.

While we have established a role for  $\alpha 7R$ -mediated suppression of DA release in NAcLat via  $LDT_{GABA} \rightarrow VTA$  activity following aversive nicotine, the mechanism underlying the increase of NAcMed DA release during the LC remains unclear; whether this increase is behaviorally relevant for nicotine aversion and which receptors mediate this effect are important topics for future studies.

With many unanswered questions about how to leverage nicotine's unique dose-dependent profile for nicotine addiction treatment in humans, the precise delineation of the neural circuitry and pharmacological mechanisms underlying nicotine aversion is a critical step toward defining novel therapeutic targets for smoking cessation pharmacotherapies.

### STAR★METHODS

Detailed methods are provided in the online version of this paper and include the following:

- **KEY RESOURCES TABLE**
- **RESOURCE AVAILABILITY**
  - Lead contact
  - Materials availability
  - Data and code availability
- **EXPERIMENTAL MODEL AND SUBJECT DETAILS**
- **METHOD DETAILS**
  - Stereotaxic surgeries
  - Jugular vein catheterization
  - Drug infusions
  - Electrophysiology
  - Fiber photometry
  - Behavioral assays
  - Computational modeling

○ Histology and microscopy  
● **QUANTIFICATION AND STATISTICAL ANALYSIS**

**SUPPLEMENTAL INFORMATION**

Supplemental information can be found online at <https://doi.org/10.1016/j.neuron.2022.07.003>.

**ACKNOWLEDGMENTS**

This work was supported by NIH (1R01DA042889), Tobacco-Related Disease Research Program (26IP-0035), One Mind Foundation (047483), NARSAD Young Investigator Award (23543), Brain Research Foundation (BRFSG-2015-7) and Wayne and Gladys Valley Foundation (all to S.L.). S.L. is a Weill Neurohub investigator, John P. Stock Faculty fellow and Rita Allen Scholar. C.L. was supported by the NSF Graduate Research Fellowship Program, Search for Hidden Figures Scholarship and HHMI Gilliam Fellowship. A.J.T. was supported by the NSF Graduate Research Fellowship Program. Experiments involving slide scanning microscopy were conducted at the CRL Molecular Imaging Center, RRID:SCR\_017852, supported by the UC Berkeley Biological Faculty Research Fund. We would like to thank Holly Aaron and Feather Ives for their microscopy advice and support. Experiments involving confocal microscopy were supported in part by the National Institutes of Health S10 program under award number 1S10RR026866-01. We thank J. Michael McIntosh for sharing a sample of  $\alpha$ -conotoxin ArlB [V11L,V16D] for preliminary experiments.

**AUTHOR CONTRIBUTIONS**

Stereotactic injections, C.L. and A.J.T.; fiber photometry, C.L., A.J.T., Y.Z., and J.W.d.J.; electrophysiology, C.L.; behavior and optogenetics, C.L. and L.W.T.; immunohistochemistry, C.L., Y.Z., and J.X.D.; critical viral reagents, K.B.T.; computational modeling, C.L. and J.P.H.V.; study design, C.L., A.J.T., and S.L.; analysis & interpretation, C.L., A.J.T., J.P.H.V., and S.L.; manuscript writing, C.L., A.J.T., and S.L.

**DECLARATION OF INTERESTS**

The authors declare no competing interests.

**INCLUSION AND DIVERSITY**

We worked to ensure sex balance in the selection of non-human subjects. One or more of the authors of this paper self-identifies as a member of the LGBTQ+ community. One or more of the authors of this paper received support from a program designed to increase minority representation in science.

Received: October 18, 2021

Revised: May 16, 2022

Accepted: July 6, 2022

Published: August 1, 2022

**REFERENCES**

Akerboom, J., Chen, T.-W., Wardill, T.J., Tian, L., Marvin, J.S., Mutlu, S., Calderón, N.C., Esposti, F., Borghuis, B.G., Sun, X.R., et al. (2012). Optimization of a GCaMP calcium indicator for neural activity imaging. *J. Neurosci.* 32, 13819–13840. <https://doi.org/10.1523/JNEUROSCI.2601-12.2012>.

Antolin-Fontes, B., Ables, J.L., Görlich, A., and Ibañez-Tallón, I. (2015). The habenulo-interpeduncular pathway in nicotine aversion and withdrawal. *Neuropharmacology* 96, 213–222. <https://doi.org/10.1016/j.neuropharm.2014.11.019>.

Ashton, H., Stepney, R., and Thompson, J.W. (1979). Self-titration by cigarette smokers. *Br. Med. J.* 2, 357–360.

Berridge, M.S., Apana, S.M., Nagano, K.K., Berridge, C.E., Leisure, G.P., and Boswell, M.V. (2010). Smoking produces rapid rise of [11C]nicotine in human brain. *Psychopharmacol. (Berl.)* 209, 383–394. <https://doi.org/10.1007/s00213-010-1809-8>.

Besson, M., David, V., Baudonnat, M., Cazala, P., Guilloux, J.P., Reperant, C., Cloez-Tayarani, I., Changeux, J.-P., Gardier, A.M., and Granon, S. (2012). Alpha7-nicotinic receptors modulate nicotine-induced reinforcement and extracellular dopamine outflow in the mesolimbic system in mice. *Psychopharmacology* 220, 1–14. <https://doi.org/10.1007/s00213-011-2422-1>.

Brischoux, F., Chakraborty, S., Brierley, D.I., and Ungless, M.A. (2009). Phasic excitation of dopamine neurons in ventral VTA by noxious stimuli. *Proc. Natl. Acad. Sci. USA* 106, 4894–4899.

Bromberg-Martin, E.S., Matsumoto, M., and Hikosaka, O. (2010). Dopamine in motivational control: rewarding, aversive, and alerting. *Neuron* 68, 815–834. <https://doi.org/10.1016/j.neuron.2010.11.022>.

Brunzell, D.H., and McIntosh, J.M. (2012). Alpha7 nicotinic acetylcholine receptors modulate motivation to self-administer nicotine: implications for smoking and schizophrenia. *Neuropsychopharmacology* 37, 1134–1143. <https://doi.org/10.1038/npp.2011.299>.

Cachope, R., Mateo, Y., Mathur, B.N., Irving, J., Wang, H.L., Morales, M., Lovinger, D.M., and Cheer, J.F. (2012). Selective activation of cholinergic interneurons enhances accumbal phasic dopamine release: setting the tone for reward processing. *Cell Rep* 2, 33–41. <https://doi.org/10.1016/j.celrep.2012.05.011>.

Coe, J.W., Brooks, P.R., Vetelino, M.G., Wirtz, M.C., Arnold, E.P., Huang, J., Sands, S.B., Davis, T.I., Lebel, L.A., Fox, C.B., et al. (2005). Varenicline: an  $\alpha 4\beta 2$  nicotinic Receptor Partial Agonist for Smoking Cessation. *J. Med. Chem.* 48, 3474–3477. <https://doi.org/10.1021/jm050069n>.

Coimbra, B., Soares-Cunha, C., Vasconcelos, N.A.P., Domingues, A.V., Borges, S., Sousa, N., and Rodrigues, A.J. (2019). Role of laterodorsal tegmentum projections to nucleus accumbens in reward-related behaviors. *Nat. Commun.* 10, 4138. <https://doi.org/10.1038/s41467-019-11557-3>.

Cunningham, C.L., and Henderson, C.M. (2000). Ethanol-induced conditioned place aversion in mice. *Behavioural Pharmacology* 11, 591–602. <https://doi.org/10.1093/00008877-200011000-00006>.

Damaj, M.I., Glassco, W., Dukat, M., and Martin, B.R. (1999). Pharmacological characterization of nicotine-induced seizures in mice. *J. Pharmacol. Exp. Ther.* 291, 1284–1291.

Dani, J.A., and Harris, R.A. (2005). Nicotine addiction and comorbidity with alcohol abuse and mental illness. *Nat. Neurosci.* 8, 1465–1470. <https://doi.org/10.1038/nn1580>.

Dautan, D., Souza, A.S., Huerta-Ocampo, I., Valencia, M., Assous, M., Witten, I.B., Deisseroth, K., Tepper, J.M., Bolam, J.P., Gerdjikov, T.V., et al. (2016). Segregated cholinergic transmission modulates dopamine neurons integrated in distinct functional circuits. *Nat. Neurosci.* 19, 1025–1033. <https://doi.org/10.1038/nn.4335>.

de Jong, J.W., Afjei, S.A., Pollak Dorocic, I., Peck, J.R., Liu, C., Kim, C.K., Tian, L., Deisseroth, K., and Lammel, S. (2019). A neural circuit mechanism for encoding aversive stimuli in the mesolimbic dopamine system. *Neuron* 101, 133–151.e7. <https://doi.org/10.1016/j.neuron.2018.11.005>.

Di Chiara, G., and Imperato, A. (1988). Drugs abused by humans preferentially increase synaptic dopamine concentrations in the mesolimbic system of freely moving rats. *Proc. Natl. Acad. Sci. USA* 85, 5274–5278. <https://doi.org/10.1073/pnas.85.14.5274>.

Erhardt, S., Schwieger, L., and Engberg, G. (2002). Excitatory and inhibitory responses of dopamine neurons in the ventral tegmental area to nicotine. *Synapse* 43, 227–237. <https://doi.org/10.1002/syn.10044>.

Ettenberg, A., Raven, M.A., Danluck, D.A., and Necessary, B.D. (1999). Evidence for opponent-process actions of intravenous cocaine. *Pharmacol. Biochem. Behav.* 64, 507–512. [https://doi.org/10.1016/s0091-3057\(99\)00109-4](https://doi.org/10.1016/s0091-3057(99)00109-4).

Fenster, C.P., Rains, M.F., Noerager, B., Quick, M.W., and Lester, R.A.J. (1997). Influence of subunit composition on desensitization of neuronal

acetylcholine receptors at low concentrations of nicotine. *J. Neurosci.* 17, 5747–5759. <https://doi.org/10.1523/JNEUROSCI.17-15-05747.1997>.

Fowler, C.D., and Kenny, P.J. (2011). Intravenous nicotine self-administration and cue-induced reinstatement in mice: effects of nicotine dose, rate of drug infusion and prior instrumental training. *Neuropharmacology* 61, 687–698. <https://doi.org/10.1016/j.neuropharm.2011.05.012>.

Fowler, C.D., and Kenny, P.J. (2014). Nicotine aversion: neurobiological mechanisms and relevance to tobacco dependence vulnerability. *Neuropharmacology* 76, 533–544. <https://doi.org/10.1016/j.neuropharm.2013.09.008>.

Fowler, C.D., Lu, Q., Johnson, P.M., Marks, M.J., and Kenny, P.J. (2011). Habenular  $\alpha 5$  nicotinic receptor subunit signalling controls nicotine intake. *Nature* 471, 597–601. <https://doi.org/10.1038/nature09797>.

Frahm, S., Šíma, M.A., Ferrarese, L., Santos-Torres, J., Antolin-Fontes, B., Auer, S., Filkin, S., Pons, S., Fontaine, J.-F., Tsetlin, V., et al. (2011). Aversion to nicotine is Regulated by the Balanced Activity of  $\beta 4$  and  $\alpha 5$  nicotinic Receptor Subunits in the Medial Habenula. *Neuron* 70, 522–535. <https://doi.org/10.1016/j.neuron.2011.04.013>.

Franklin, K.B.J., and Paxinos, G. (2013). *Paxinos and Franklin's The mouse brain in stereotaxic coordinates* (Academic Press).

Fudala, P.J., and Iwamoto, E.T. (1990). Conditioned aversion after delay place conditioning with amphetamine. *Pharmacology Biochemistry and Behavior* 35, 89–92. [https://doi.org/10.1016/0091-3057\(90\)90209-Z](https://doi.org/10.1016/0091-3057(90)90209-Z).

Fudala, P.J., and Iwamoto, E.T. (1987). Conditioned aversion after delay place conditioning with nicotine. *Psychopharmacology* 92, 376–381. <https://doi.org/10.1007/BF00210847>.

Fudala, P.J., Teoh, K.W., and Iwamoto, E.T. (1985). Pharmacologic characterization of nicotine-induced conditioned place preference. *Pharmacol. Biochem. Behav.* 22, 237–241. [https://doi.org/10.1016/0091-3057\(85\)90384-3](https://doi.org/10.1016/0091-3057(85)90384-3).

Gao, M., Jin, Y., Yang, K., Zhang, D., Lukas, R.J., and Wu, J. (2010). Mechanisms involved in systemic nicotine-induced glutamatergic synaptic plasticity on dopamine neurons in the ventral tegmental area. *J. Neurosci.* 30, 13814–13825. <https://doi.org/10.1523/JNEUROSCI.1943-10.2010>.

Goldberg, S.R., Spealman, R.D., Risner, M.E., and Henningfield, J.E. (1983). Control of behavior by intravenous nicotine injections in laboratory animals. *Pharmacol. Biochem. Behav.* 19, 1011–1020. [https://doi.org/10.1016/0091-3057\(83\)90408-2](https://doi.org/10.1016/0091-3057(83)90408-2).

Goldstein, N., Carty, J.R.E., and Betley, J.N. (2022). Specificity of varenicline in blocking mesolimbic circuit activation to natural and drug rewards. *Neuroscience* 483, 40–51. <https://doi.org/10.1016/j.neuroscience.2021.12.016>.

Graupner, M., Maex, R., and Gutkin, B. (2013). Endogenous cholinergic inputs and local circuit mechanisms govern the phasic mesolimbic dopamine response to nicotine. *PLoS Comput. Biol.* 9, e1003183. <https://doi.org/10.1371/journal.pcbi.1003183>.

Grieder, T.E., Besson, M., Maal-Bared, G., Pons, S., Maskos, U., and van der Kooy, D. (2019).  $\beta 2^*$  NAcHRs on VTA dopamine and GABA neurons separately mediate nicotine aversion and reward. *Proc. Natl. Acad. Sci. USA* 116, 25968–25973. <https://doi.org/10.1073/pnas.1908724116>.

Grottick, A.J., Trube, G., Corrigall, W.A., Huwyler, J., Malherbe, P., Wyler, R., and Higgins, G.A. (2000). Evidence that nicotinic  $\alpha 7$  receptors are not involved in the hyperlocomotor and rewarding effects of nicotine. *J. Pharmacol. Exp. Ther.* 294, 1112–1119.

Harenza, J.L., Muldoon, P.P., De Biasi, M., Damaj, M.I., and Miles, M.F. (2014). Genetic variation within the *Chrna7* gene modulates nicotine reward-like phenotypes in mice. *Genes Brain Behav.* 13, 213–225. <https://doi.org/10.1111/gbb.12113>.

Heishman, S.J., and Henningfield, J.E. (2000). Tolerance to repeated nicotine administration on performance, subjective, and physiological responses in nonsmokers. *Psychopharmacology* 152, 321–333. <https://doi.org/10.1007/s002130000541>.

Hnasko, T.S., Sotak, B.N., and Palmiter, R.D. (2007). Cocaine-conditioned place preference by dopamine-deficient mice is mediated by serotonin. *J. Neurosci.* 27, 12484–12488. <https://doi.org/10.1523/JNEUROSCI.3133-07.2007>.

Hsu, Y.-W., Tempest, L., Quina, L.A., Wei, A.D., Zeng, H., and Turner, E.E. (2013). Medial habenula output circuit mediated by 5 nicotinic receptor-expressing GABAergic neurons in the interpeduncular nucleus. *J. Neurosci.* 33, 18022–18035. <https://doi.org/10.1523/JNEUROSCI.2927-13.2013>.

Imperato, A., Mulas, A., and Di Chiara, G. (1986). Nicotine preferentially stimulates dopamine release in the limbic system of freely moving rats. *Eur. J. Pharmacol.* 132, 337–338. [https://doi.org/10.1016/0014-2999\(86\)90629-1](https://doi.org/10.1016/0014-2999(86)90629-1).

Klink, R., de Kerchove d'Exaerde, A.de K., Zoli, M., and Changeux, J.P. (2001). Molecular and physiological diversity of nicotinic acetylcholine receptors in the midbrain dopaminergic nuclei. *J. Neurosci.* 21, 1452–1463. <https://doi.org/10.1523/JNEUROSCI.21-05-01452.2001>.

Kmiotek, E.K., Baimel, C., and Gill, K.J. (2012). Methods for intravenous self-administration in a mouse model. *J. Vis. Exp.* 70, e3739. <https://doi.org/10.3791/3739>.

Kohlmeier, K.A. (2013). Off the beaten path: drug addiction and the pontine lat-erodorsal tegmentum. *ISRN Neurosci* 2013, 604847. <https://doi.org/10.1155/2013/604847>.

Lachenmeier, D.W., and Rehm, J. (2015). Comparative risk assessment of alcohol, tobacco, cannabis and other illicit drugs using the margin of exposure approach. *Sci. Rep.* 5, 8126. <https://doi.org/10.1038/srep08126>.

Lammel, S., Lim, B.K., Ran, C., Huang, K.W., Betley, M.J., Tye, K.M., Deisseroth, K., and Malenka, R.C. (2012). Input-specific control of reward and aversion in the ventral tegmental area. *Nature* 491, 212–217. <https://doi.org/10.1038/nature11527>.

Laviolette, S.R., and van der Kooy, D. (2003). The motivational valence of nicotine in the rat ventral tegmental area is switched from rewarding to aversive following blockade of the  $\alpha 7$ -subunit-containing nicotinic acetylcholine receptor. *Psychopharmacol. (Berl.)* 166, 306–313. <https://doi.org/10.1007/s00213-002-1317-6>.

Laviolette, S.R., and van der Kooy, D. (2004). The neurobiology of nicotine addiction: bridging the gap from molecules to behaviour. *Nat. Rev. Neurosci.* 5, 55–65. <https://doi.org/10.1038/nrn1298>.

Loney, G.C., King, C.P., and Meyer, P.J. (2021). Systemic nicotine enhances opioid self-administration and modulates the formation of opioid-associated memories partly through actions within the insular cortex. *Sci. Rep.* 11, 3321. <https://doi.org/10.1038/s41598-021-81955-5>.

Lowes, D.C., Chamberlin, L.A., Kretsga, L.N., Holt, E.S., Abbas, A.I., Park, A.J., Yusufova, L., Bretton, Z.H., Firdous, A., Enikolopov, A.G., et al. (2021). Ventral tegmental area GABA neurons mediate stress-induced blunted reward-seeking in mice. *Nat. Commun.* 12, 3539. <https://doi.org/10.1038/s41467-021-23906-2>.

Lüscher, C., and Malenka, R.C. (2011). Drug-evoked synaptic plasticity in addiction: from molecular changes to circuit remodeling. *Neuron* 69, 650–663. <https://doi.org/10.1016/j.neuron.2011.01.017>.

Mameli-Engvall, M., Evrard, A., Pons, S., Maskos, U., Svensson, T.H., Changeux, J.P., and Faure, P. (2006). Hierarchical control of dopamine neuron-firing patterns by nicotinic receptors. *Neuron* 50, 911–921. <https://doi.org/10.1016/j.neuron.2006.05.007>.

Mansvelder, H.D., Keath, J.R., and McGehee, D.S. (2002). Synaptic mechanisms underlie nicotine-induced excitability of brain reward areas. *Neuron* 33, 905–919. [https://doi.org/10.1016/S0896-6273\(02\)00625-6](https://doi.org/10.1016/S0896-6273(02)00625-6).

Mansvelder, H.D., and McGehee, D.S. (2000). Long-term potentiation of excitatory inputs to brain reward areas by nicotine. *Neuron* 27, 349–357. [https://doi.org/10.1016/S0896-6273\(00\)00042-8](https://doi.org/10.1016/S0896-6273(00)00042-8).

Markou, A., and Paterson, N.E. (2001). The nicotinic antagonist methyllycyclohexylamine has differential effects on nicotine self-administration and nicotine withdrawal in the rat. *Nicotine Tob. Res.* 3, 361–373. <https://doi.org/10.1080/14622200110073380>.

Matta, S.G., Balfour, D.J., Benowitz, N.L., Boyd, R.T., Buccafusco, J.J., Caggiula, A.R., Craig, C.R., Collins, A.C., Damaj, M.I., Donny, E.C., et al. (2007). Guidelines on nicotine dose selection for *in vivo* research. *Psychopharmacology* 190, 269–319. <https://doi.org/10.1007/s00213-006-0441-0>.

McCauley, M.E., Wand, G.S., Kuwabara, H., Dannals, R.F., Wong, D., and Xu, X. (2020). The Relationship of Varenicline Agonism of  $\alpha 4\beta 2$  nicotinic acetylcholine Receptors and nicotine-Induced dopamine Release in nicotine-Dependent Humans. *Nicotine Tob. Res.* 22, 892–899. <https://doi.org/10.1093/nter/ntz080>.

Mihalak, K.B., Carroll, F.I., and Luetje, C.W. (2006). Varenicline is a partial agonist at alpha4beta2 and a full agonist at alpha7 neuronal nicotinic receptors. *Mol. Pharmacol.* 70, 801–805. <https://doi.org/10.1124/mol.106.025130>.

Natarajan, R., Wright, J.W., and Harding, J.W. (2011). Nicotine-induced conditioned place preference in adolescent rats. *Pharmacol. Biochem. Behav.* 99, 519–523. <https://doi.org/10.1016/j.pbb.2011.05.004>.

Nguyen, C., Mondoloni, S., Le Borgne, T., Centeno, I., Come, M., Jehl, J., Solié, C., Reynolds, L.M., Durand-de Cottoli, R., Tolu, S., et al. (2021). Nicotine inhibits the VTA-to-amygdala dopamine pathway to promote anxiety. *Neuron* 109, 2604–2615.e9. <https://doi.org/10.1016/j.neuron.2021.06.013>.

Omelchenko, N., and Sesack, S.R. (2005). Laterodorsal tegmental projections to identified cell populations in the rat ventral tegmental area. *J. Comp. Neurol.* 483, 217–235. <https://doi.org/10.1002/cne.20417>.

Petersen, D.R., Norris, K.J., and Thompson, J.A. (1984). A comparative study of the disposition of nicotine and its metabolites in three inbred strains of mice. *Drug Metab. Dispos.* 12, 725–731.

Picciotto, M.R., Addy, N.A., Mineur, Y.S., and Brunzell, D.H. (2008). It's not "either/or": activation and desensitization of nicotinic acetylcholine receptors both contribute to behaviors related to nicotine addiction and mood. *Prog. Neurobiol.* 84, 329–342. <https://doi.org/10.1016/j.pneurobio.2007.12.005>.

Picciotto, M.R., and Kenny, P.J. (2021). Mechanisms of nicotine addiction. *Cold Spring Harb. Perspect. Med.* 11, a039610. <https://doi.org/10.1101/cshperspect.a039610>.

Picciotto, M.R., Zoli, M., Rimondini, R., Léna, C., Marubio, L.M., Pich, E.M., Fuxé, K., and Changeux, J.P. (1998). Acetylcholine receptors containing the  $\beta 2$  subunit are involved in the reinforcing properties of nicotine. *Nature* 391, 173–177. <https://doi.org/10.1038/34413>.

Rice, M.E., and Cragg, S.J. (2004). Nicotine amplifies reward-related dopamine signals in striatum. *Nat. Neurosci.* 7, 583–584. <https://doi.org/10.1038/nn1244>.

Risinger, F.O., and Oakes, R.A. (1995). Nicotine-induced conditioned place preference and conditioned place aversion in mice. *Pharmacol. Biochem. Behav.* 51, 457–461. [https://doi.org/10.1016/0091-3057\(95\)00007-J](https://doi.org/10.1016/0091-3057(95)00007-J).

Saal, D., Dong, Y., Bonci, A., and Malenka, R.C. (2003). Drugs of abuse and stress trigger a common synaptic adaptation in dopamine neurons. *Neuron* 37, 577–582. [https://doi.org/10.1016/s0896-6273\(03\)00021-7](https://doi.org/10.1016/s0896-6273(03)00021-7).

Sambo, D.O., Lin, M., Owens, A., Lebowitz, J.J., Richardson, B., Jagnarine, D.A., Shetty, M., Rodriguez, M., Alonge, T., Ali, M., et al. (2017). The sigma-1 receptor modulates methamphetamine dysregulation of dopamine neuro-transmission. *Nat. Commun.* 8, 2228. <https://doi.org/10.1038/s41467-017-02087-x>.

Sartor, C.E., Lessov-Schlaggar, C.N., Scherrer, J.F., Bucholz, K.K., Madden, P.A.F., Pergadia, M.L., Grant, J.D., Jacob, T., and Xian, H. (2010). Initial response to cigarettes predicts rate of progression to regular smoking: findings from an offspring-of-twins design. *Addict. Behav.* 35, 771–778. <https://doi.org/10.1016/j.addbeh.2010.03.004>.

Schilström, B., Rawal, N., Mameli-Engvall, M., Nomikos, G.G., and Svensson, T.H. (2003). Dual effects of nicotine on dopamine neurons mediated by different nicotinic receptor subtypes. *Int. J. Neuropsychopharmacol.* 6, 1–11. <https://doi.org/10.1017/S1461145702003188>.

Schultz, W. (1997). Dopamine neurons and their role in reward mechanisms. *Curr. Opin. Neurobiol.* 7, 191–197.

Sellings, L.H.L., Baharnouri, G., McQuade, L.E., and Clarke, P.B.S. (2008). Rewarding and aversive effects of nicotine are segregated within the nucleus accumbens. *Eur. J. Neurosci.* 28, 342–352. <https://doi.org/10.1111/j.1460-9568.2008.06341.x>.

Siu, E.C.K., and Tyndale, R.F. (2007). Characterization and comparison of nicotine and cotinine metabolism in vitro and in vivo in DBA/2 and C57BL/6 mice. *Mol. Pharmacol.* 71, 826–834. <https://doi.org/10.1124/mol.106.032086>.

Soden, M.E., Chung, A.S., Cuevas, B., Resnick, J.M., Awatramani, R., and Zweifel, L.S. (2020). Anatomic resolution of neurotransmitter-specific projections to the VTA reveals diversity of GABAergic inputs. *Nat. Neurosci.* 23, 968–980. <https://doi.org/10.1038/s41593-020-0657-z>.

St Helen, G., Ross, K.C., Dempsey, D.A., Havel, C.M., Jacob, P., and Benowitz, N.L. (2016). Nicotine delivery and vaping behavior During ad libitum E-cigarette access. *Tob. Regul. Sci.* 2, 363–376. <https://doi.org/10.18001/TRS.2.4.8>.

Steidl, S., Wang, H., Ordonez, M., Zhang, S., and Morales, M. (2017). Optogenetic excitation in the ventral tegmental area of glutamatergic or cholinergic inputs from the laterodorsal tegmental area drives reward. *Eur. J. Neurosci.* 45, 559–571. <https://doi.org/10.1111/ejn.13436>.

Tan, K.R., Yvon, C., Turiault, M., Mirzabekov, J.J., Doehner, J., Labouébe, G., Deisseroth, K., Tye, K.M., and Lüscher, C. (2012). GABA neurons of the VTA drive conditioned place aversion. *Neuron* 73, 1173–1183. <https://doi.org/10.1016/j.neuron.2012.02.015>.

Tapper, A.R., McKinney, S.L., Nashmi, R., Schwarz, J., Deshpande, P., Labarca, C., Whiteaker, P., Marks, M.J., Collins, A.C., and Lester, H.A. (2004). Nicotine Activation of  $\alpha 4^*$  Receptors: sufficient for Reward, Tolerance, and Sensitization. *Science* 306, 1029–1032. <https://doi.org/10.1126/science.1099420>.

Taylor, D.H., Burman, P.N., Hansen, M., Wilcox, R.S., Larsen, B.R., Blanchard, J.K., Merrill, C., Edwards, J., Sudweeks, S., Wu, J., et al. (2013). Nicotine enhances the excitability of GABA neurons in the ventral Tegmental Area via activation of alpha 7 nicotinic receptors on glutamate terminals. *Biochem. Pharmacol.* S1–007, 1–9. <https://doi.org/10.4172/2167-0501.S1-002>.

Threlfell, S., Lalic, T., Platt, N.J., Jennings, K.A., Deisseroth, K., and Cragg, S.J. (2012). Striatal dopamine release is triggered by synchronized activity in cholinergic interneurons. *Neuron* 75, 58–64. <https://doi.org/10.1016/j.neuron.2012.04.038>.

Tolu, S., Eddine, R., Marti, F., David, V., Graupner, M., Pons, S., Baudonnat, M., Husson, M., Besson, M., Reperant, C., et al. (2013). Co-activation of VTA DA and GABA neurons mediates nicotine reinforcement. *Mol. Psychiatry* 18, 382–393. <https://doi.org/10.1038/mp.2012.83>.

Tsai, H.-C., Zhang, F., Adamantidis, A., Stuber, G.D., Bonci, A., de Lecea, L., and Deisseroth, K. (2009). Phasic firing in dopaminergic neurons is sufficient for behavioral conditioning. *Science* 324, 1080–1084. <https://doi.org/10.1126/science.1168878>.

Tuesta, L.M., Chen, Z., Duncan, A., Fowler, C.D., Ishikawa, M., Lee, B.R., Liu, X.-A., Lu, Q., Cameron, M., Hayes, M.R., et al. (2017). GLP-1 acts on habenular avoidance circuits to control nicotine intake. *Nat. Neurosci.* 20, 708–716. <https://doi.org/10.1038/nn.4540>.

Verharen, J.P.H., Zhu, Y., and Lammel, S. (2020). Aversion hot spots in the dopamine system. *Curr. Opin. Neurobiol.* 64, 46–52. <https://doi.org/10.1016/j.conb.2020.02.002>.

Wang, H.-L., and Morales, M. (2009). Pedunculopontine and laterodorsal tegmental nuclei contain distinct populations of cholinergic, glutamatergic and GABAergic neurons in the rat. *Eur. J. Neurosci.* 29, 340–358. <https://doi.org/10.1111/j.1460-9568.2008.06576.x>.

Weissbourd, B., Ren, J., DeLoach, K.E., Guenther, C.J., Miyamichi, K., and Luo, L. (2014). Presynaptic partners of dorsal raphe serotonergic and GABAergic neurons. *Neuron* 83, 645–662. <https://doi.org/10.1016/j.neuron.2014.06.024>.

Whiteaker, P., Christensen, S., Yoshikami, D., Dowell, C., Watkins, M., Gulyas, J., Rivier, J., Olivera, B.M., and McIntosh, J.M. (2007). Discovery, Synthesis, and Structure Activity of a Highly Selective  $\alpha 7$  nicotinic acetylcholine

Receptor Antagonist. *Biochemistry* 46, 6628–6638. <https://doi.org/10.1021/bi7004202>.

Wilson, R.C., and Collins, A.G. (2019). Ten simple rules for the computational modeling of behavioral data. *eLife* 8, e49547. <https://doi.org/10.7554/eLife.49547>.

Wolfman, S.L., Gill, D.F., Bogdanic, F., Long, K., Al-Hasani, R., McCall, J.G., Bruchas, M.R., and McGehee, D.S. (2018). Nicotine aversion is mediated by GABAergic interpeduncular nucleus inputs to laterodorsal tegmentum. *Nat. Commun.* 9, 2710. <https://doi.org/10.1038/s41467-018-04654-2>.

Wooltorton, J.R.A., Pidoplichko, V.I., Broide, R.S., and Dani, J.A. (2003). Differential desensitization and distribution of nicotinic acetylcholine receptor subtypes in midbrain dopamine areas. *J. Neurosci.* 23, 3176–3185. <https://doi.org/10.1523/JNEUROSCI.23-08-03176.2003>.

Yang, C.F., Chiang, M.C., Gray, D.C., Prabhakaran, M., Alvarado, M., Juntti, S.A., Unger, E.K., Wells, J.A., and Shah, N.M. (2013). Sexually dimorphic neurons in the ventromedial hypothalamus govern mating in both sexes and aggression in males. *Cell* 153, 896–909. <https://doi.org/10.1016/j.cell.2013.04.017>.

Yang, H., Yang, J., Xi, W., Hao, S., Luo, B., He, X., Zhu, L., Lou, H., Yu, Y.Q., Xu, F., et al. (2016). Laterodorsal tegmentum interneuron subtypes oppositely regulate olfactory cue-induced innate fear. *Nat. Neurosci.* 19, 283–289. <https://doi.org/10.1038/nn.4208>.

## STAR★METHODS

### KEY RESOURCES TABLE

REAGENT or RESOURCE	SOURCE	IDENTIFIER
<b>Chemicals</b>		
CNQX	Tocris	CAS: 479347-85-8
D-AP5	Fisher Scientific	Cat#: 01-061-00
TTX	Hello Bio	Cat#: HB1035
4-AP	Sigma-Aldrich	CAS: 504-24-5
Red retrobeads IX	Lumafluor	Item#: R170
(-)-Nicotine detartrate	Tocris	CAS: 65-31-6
Methyllycaconitine citrate salt	Millipore Sigma	CAS: 112825-05-5
Mecamylamine hydrochloride	Sigma-Aldrich	CAS: 826-39-1
Dihydro-b-erythroidine hydrobromide	Tocris	CAS: 29734-68-7
<b>Fluorescent <i>in situ</i> hybridization with RNAscope®</b>		
RNAscope® Multiplex Fluorescent Reagent Kit v2	Advanced Cell Diagnostics	Cat#: 323100
RNAscope® Probe – Mm-Gad2 – <i>Mus musculus</i> glutamic acid decarboxylase 2 (Gad2) mRNA	Advanced Cell Diagnostics	Cat#: 439371
RNAscope® Probe - Mm-Chrna7-C2 - <i>Mus musculus</i> cholinergic receptor nicotinic alpha polypeptide 7 (Chrna7) mRNA	Advanced Cell Diagnostics	Cat#: 465161-C2
Opal 520 Reagent Pack	Akoya Biosciences	Cat#: FP1487001KT
Opal 570 Reagent Pack	Akoya Biosciences	Cat#: FP1488001KT
<b>Antibodies</b>		
Goat anti-mouse Alexa-Fluor 488	Thermo Fisher Scientific	RRID: AB_2534069
Rabbit anti-tyrosine hydroxylase	Millipore	RRID: AB_390204
Mouse anti-tyrosine hydroxylase	Millipore	RRID: AB_2201528
Goat anti-mouse Alexa Fluor 546	Thermo Fisher Scientific	RRID: AB_2534071
Goat anti-rabbit Alexa Fluor 488	Thermo Fisher Scientific	RRID: AB_228341
Goat anti-mouse Alexa Fluor 647	Thermo Fisher Scientific	RRID: AB_2535804
Anti-Digoxigenin-AP FAB fragments	Roche	RRID: AB_514497
Chicken anti-GFP	Abcam	RRID: AB_300798
Goat anti-chicken Alexa Fluor 488	Abcam	RRID: AB_2636803
<b>Experimental Models: Organisms/Strains</b>		
C57BL/6J	The Jackson Laboratory	RRID: IMSR_JAX:000664
DAT::IRES-Cre	The Jackson Laboratory	RRID: IMSR_JAX: 006660
VGLUT2::IRES-Cre	The Jackson Laboratory	RRID: IMSR_JAX: 016963

(Continued on next page)

**Continued**

REAGENT or RESOURCE	SOURCE	IDENTIFIER
GAD2::IRES-Cre	The Jackson Laboratory	RRID: IMSR_JAX: 010802
<b>Bacterial and Virus Strains</b>		
AAV-EF1a-DIO-hChR2(H134R)-eYFP	UNC Vector Core	N/A
AAV-EF1a-DIO-eYFP	UNC Vector Core	N/A
AAV5-EF1 $\alpha$ -DIO-mCherry	UNC Vector Core	N/A
AAVDJ-DIO-GCaMP6m	UNC Vector Core	N/A
AAV-EF1a-FLEX-TVA-mCherry	UNC Vector Core	N/A
AAV-CA-FLEX-RG	UNC Vector Core	N/A
Rabies EnvA- $\Delta$ G-GFP	Kevin Beier	N/A
AAV5-hSyn-dLight1.2	Addgene	N/A
AAV8.2-hEF1a-DIO-synaptophysin-eYFP	MIT Vector Core	N/A
AAV5-flex-taCasp3-TEVp	UNC Vector Core	N/A
AAV9-hSyn1-FLEX-axon-GCaMP6s	Addgene	N/A
AAV-EF1a-DIO-eNpHR3.0-eYFP	UNC Vector Core	N/A

**RESOURCE AVAILABILITY**

**Lead contact**

Further information and requests for resources and reagents should be directed to and will be fulfilled by the lead contact, Stephan Lammel ([lammel@berkeley.edu](mailto:lammel@berkeley.edu)).

**Materials availability**

This study did not generate new unique reagents.

**Data and code availability**

The datasets generated during and/or analyzed during the current study are available from the [lead contact](#) upon reasonable request. All custom code used for analysis in this study is available from the [lead contact](#) upon reasonable request. Any additional information required to reanalyze the data reported in this work paper is available from the [lead contact](#) upon request.

**EXPERIMENTAL MODEL AND SUBJECT DETAILS**

The following mouse lines (20–35g, 8–20 weeks old, males and females were counterbalanced across conditions with no significant effects of sex observed) were used for experiments: C57BL/6J mice (Jackson Laboratory, stock number: 000664), DAT::IRES-Cre (Jackson Laboratory, stock number: 006660, strain code: B6.SJL-Slc6a3tm1.1(cre)Bkmn/J), VGLUT2::IRES-Cre (Jackson Laboratory, stock number: 016963, strain code: Slc17a6tm2(cre)LowJ/J), and GAD2::IRES-Cre (Jackson Laboratory, stock number: 010802, strain code: Gad2tm2(cre)Zjh/J). All lines have been crossed onto the C57BL/6J background for at least six generations. Mice were maintained on a 12:12 light cycle (lights on at 07:00). All procedures complied with the animal care standards set forth by the National Institutes of Health and were approved by University of California, Berkeley's Administrative Panel on Laboratory Animal Care.

**METHOD DETAILS**

**Stereotaxic surgeries**

As previously described (Lammel et al., 2012), all stereotaxic injections were performed under general ketamine–dexmedetomidine anesthesia and using a stereotaxic instrument (Kopf Instruments and Model 1900). For red fluorescent retrograde labeling, mice were injected unilaterally with fluorescent retrobeads (100 nl; LumaFluor Inc.) in the nucleus accumbens (NAc) lateral shell (NAcLat; bregma: 0.98 mm, lateral: 2 mm, ventral: –4.2 mm) or ventral tegmental area (VTA; bregma: –3.4 mm, lateral: 0.3 mm, ventral: –4.5 mm) using a 1  $\mu$ l Hamilton syringe (Hamilton). The AAVs (adenovirus) used in this study were from the Deisseroth laboratory (AAV5-EF1 $\alpha$ -DIO-hChR2(H134R)-eYFP; AAV5-EF1 $\alpha$ -DIO-eYFP; AAV5-EF1 $\alpha$ -DIO-mCherry; AAVDJ-DIO-GCaMP6m; AAV-EF1a-DIO-eNpHR3.0-eYFP  $\sim$ 10<sup>12</sup> infectious units per ml, prepared by the University of North Carolina Vector Core Facility), from the Uchida lab (Harvard) (AAV5-flex-RG; AAV5-flex-TVA-mCherry;  $\sim$ 10<sup>12</sup> infectious units per ml; prepared by the University of North Carolina Vector Core Facility), from the Tian Lab (UC Davis) (AAV5-hSyn-dLight1.2; AAV9-hSyn1-FLEX-axon-GCaMP6s; prepared by Addgene), from the MIT Vector Core (AAV8.2-hEF1a-DIO-synaptophysin-eYFP), or from the Shah

lab (UCSF) (AAV5-flex-taCasp3-TEVp;  $\sim 10^{12}$  infectious units per ml; prepared by the University of North Carolina Vector Core Facility). RV-EnvA- $\Delta$ G-GFP was from Kevin Beier (UC Irvine), and 300 nl concentrated virus solution was injected into the VTA (same coordinates as above). For AAV viral injections, 100–500 nl of concentrated AAV solution was injected into the ventral NAc medial shell (NAcMed; bregma: 1.5 mm, lateral: 0.9 mm, ventral: -4.8 mm) and/or NAcLat (same coordinates as above), VTA (same coordinates as above), or laterodorsal tegmentum (LDT; bregma: -5 mm, lateral: 0.5 mm, ventral: -3.4 mm) using a syringe pump (Harvard Apparatus) at 150 nl/min. The injection needle was withdrawn 5 min after the end of the infusion. For behavioral experiments, animals injected with Cre-dependent Channelrhodopsin-2 (ChR2) or eYFP received unilateral implantation of a chronically implanted optical fiber (400  $\mu$ m, NA = 0.48; Doric Lenses Inc.) dorsal to the VTA (bregma: -3.4 mm, lateral: 0.3 mm, ventral: -3.9 mm). For *in vivo* fiber photometry experiments, mice received unilateral implantation of a chronically implanted optical fiber (400  $\mu$ m, NA = 0.48; Doric Lenses Inc.) in the VTA (same coordinates as above or angled at 15 degrees with bregma: -3.4 mm, lateral: 1.5 mm, ventral: -4.65 mm) or dual optical fibers in the NAcMed and NAcLat (same coordinates as above) of the same animal. One layer of adhesive cement (C&B Metabond; Parkell) followed by cranioplastic cement (Dental cement) was used to secure the fiber to the skull. The incision was closed with a suture and tissue adhesive (Vetbond; 3M). The animal was woken up with an I.P. injection of atipamezole and kept on a heating pad until it recovered from anesthesia. Experiments were performed 2–12 weeks (for AAVs) or 2–7 days (for retrobeads or rabies) after stereotactic injection. Injection sites and optical fiber placements were confirmed in all animals by preparing coronal sections (50–100  $\mu$ m) of injection and implantation sites.

### **Jugular vein catheterization**

The protocol for surgical implantation of a catheter in the jugular vein was adapted from Kmiotek et al. (2012). Briefly, animals were anesthetized with 1:1 ketamine–dexmedetomidine and their temperature maintained on a heating pad for the duration of the surgery. A 4 cm long polyurethane catheter (Silastic) with a silicone bulb 1 cm from the insertion end and a modified, blunted syringe tip on the infusion end was inserted into the jugular vein. After checking for patency, the catheter was secured to the jugular vein with knots made by sutures above and below the silicone bulb. The chest incision was closed with dissolvable sutures and tissue adhesive. The infusion end of the catheter was capped and cemented to the skull with adhesive cement (C&B Metabond; Parkell) followed by cranioplastic cement (dental cement). Mice were kept on a heating pad until recovered from anesthesia. Catheters were flushed daily with physiological saline, and heparin was infused to prevent clogging if necessary. Experiments were performed 2 days after jugular vein catheterization. Patency was verified after experiments were completed via infusion of sodium pentobarbital.

### **Drug infusions**

For nicotine infusion experiments, animals were infused with a total of 0.25 mg/kg or 1.25 mg/kg nicotine (free-base) dissolved in sterile, physiological 0.9% saline. Animals received infusions at a volume of 1.25  $\mu$ l/g (41  $\mu$ g/kg nicotine per infusion for 0.25 mg/kg total or 208  $\mu$ g/kg/inf for 1.25 mg/kg total) six times over 30 minutes, every five minutes, through the jugular vein catheter. For fiber photometry experiments, animals were head-fixed on a running wheel and then underwent a 10-minute baseline recording session before the initiation of the same nicotine infusion protocol as shown in Figure 1A. In experiments involving nAChR antagonists, animals received a pre-treatment infusion of the antagonist or saline at minute 5 during the 10-minute baseline recording. nAChR antagonists were then co-infused with aversive nicotine according to the protocol described above starting at minute 10. Animals received aversive nicotine with MEC (1.1 mg/kg), MLA (4.5 mg/kg), DHBE (3 mg/kg, except GAD2-Cre animals, which received 1.7 mg/kg due to high fatality rates) or without antagonist on separate recording days with 48 hours between each session. Antagonist solutions were prepared in physiological saline to achieve free base doses at a volume of 1.25  $\mu$ l/g/infusion whether delivered alone during the minute 5 pre-treatment or co-infused with 1.25 mg/kg free base nicotine

### **Electrophysiology**

Mice were deeply anaesthetized with pentobarbital (200 mg/kg ip; Vortech). Coronal midbrain slices (200  $\mu$ m) were prepared after intracardial perfusion with ice-cold artificial cerebrospinal fluid (ACSF) containing (in mM) 50 sucrose, 125 NaCl, 25 NaHCO<sub>3</sub>, 2.5 KCl, 1.25 NaH<sub>2</sub>PO<sub>4</sub>, 0.1 CaCl<sub>2</sub>, 4.9 MgCl<sub>2</sub>, and 2.5 glucose (oxygenated with 95% O<sub>2</sub>/5% CO<sub>2</sub>). After 90 min of recovery, slices were transferred to a recording chamber and perfused continuously at 2–4 ml/min with oxygenated ACSF, containing (in mM) 125 NaCl, 25 NaHCO<sub>3</sub>, 2.5 KCl, 1.25 NaH<sub>2</sub>PO<sub>4</sub>, 11 glucose, 1.3 MgCl<sub>2</sub> and 2.5 CaCl<sub>2</sub> at  $\sim$ 30 °C. Cells were visualized with a 40x water-immersion objective on an upright fluorescent microscope (BX51WI; Olympus) equipped with infrared-differential interference contrast video microscopy and epifluorescence (Olympus). Patch pipettes (3.8–4.4 M $\Omega$ ) were pulled from borosilicate glass (G150TF-4; Warner Instruments) and filled with internal solution, which consisted of (in mM) 130 CsCl, 1 EGTA, 10 HEPES, 1 MgATP, 0.2 NaGTP, 0.1% neurobiotin pH 7.35 (270–285 mOsm). Light-evoked IPSCs (Figures 5A–5D) were recorded in the presence of 20  $\mu$ M CNQX (6-cyano-7-nitroquinoxaline-2,3-dione, Bio-tech) and 50  $\mu$ M D-AP5 (Tocris) to block AMPA and NMDA receptors, respectively. We also added the voltage-gated sodium channel antagonist tetrodotoxin (TTX, 1  $\mu$ M, Hello Bio) and the potassium channel antagonist 4-aminopyridine (4-AP, 1 mM, Sigma) to the bath solution in order to isolate monosynaptic inputs. Electrophysiological recordings were made at 32 °C using a MultiClamp700B amplifier and acquired using a Digidata 1440A digitizer, sampled at 10 kHz, and filtered at 2 kHz. All data acquisition was performed using pCLAMP software (Molecular Devices). Channelrhodopsin-2 was stimulated by flashing 473 nm light through the light path of the microscope using an ultrahigh-powered light-emitting diode (LED) powered by an LED driver (Prizmatix) under computer control. A dual lamp house adaptor (Olympus) was used to switch

between fluorescence lamp and LED light source. The light intensity of the LED was not changed during the experiments and the whole slice was illuminated (5 mW/mm<sup>2</sup>). Light-evoked IPSCs were obtained every 20 s with one pulse of 473 nm wavelength light (3 ms) with neurons voltage clamped at -70 mV. Series resistance (15–25 MΩ) and input resistance were monitored online. Data were analyzed offline using Clampfit (Molecular Devices) or IgorPro Software (Wavemetrics). Light-evoked IPSC amplitudes were calculated by averaging responses from 10 sweeps and then measuring the peak amplitude in a 50 ms window after the light pulse. Cells that did not show a peak in this window that exceeded the baseline noise were counted as non-responders. To determine the dopaminergic identity of retrobead-labeled VTA neurons (i.e., tyrosine hydroxylase (TH)-immunopositive or TH-immunonegative), cells were filled with neurobiotin (Vector) during patch clamp recordings, then fixed in 4% paraformaldehyde (PFA) and 24 h later immunostained for TH. All recorded retrobead-labeled cells were located in the lateral VTA and were TH-immunopositive.

### Fiber photometry

Four to eight weeks after virus injection, animals were implanted with fiberoptic implants and/or jugular vein catheters and allowed to recover for 2–7 days before fiber photometry recordings. In experiments with dual fiberoptic implants (Figures 3 and 6), animals were implanted in one NAc subregion on one side, and the other region on the other side, sides counterbalanced between animals. For experiments involving IV infusions, a baseline of 10 minutes was recorded in head-fixed animals before initiating intravenous nicotine infusions (same protocol as shown in Figure 1A) with antagonist infusion at minute 5 for experiments involving antagonists (see ‘DRUG INFUSIONS’ section above for dose and timing protocols). In experiment involving ChR2 stimulation of LDT<sub>GABA</sub> neurons (Figures 5E–5G), animals received 3–5mW 473 nm laser stimulation over 2 s (5 ms pulses at 20 Hz) every 10 s for a total of 20 trials per session. Calcium or DA transients were measured in head-fixed animals using a custom-built fiber photometry system as described previously (de Jong et al., 2019). Briefly, fluorescence signals were obtained by stimulating cells expressing GCaMP6m, GCaMP6s, or dLight1.2 with a 470 nm LED (20 μW at fiber tip) while calcium-independent signals were obtained by stimulating these cells with a 405 nm LED (20 μW at fiber tip). 470 nm and 405 nm LED light were alternated at 20 Hz and light emission was recorded using an sCMOS Camera (Hamamatsu Flash or Photometrics Prime), which acquired video frames containing the entire fiber bundle (2 fibers, 3 m in length, NA = 0.48, 400 μm core, Doric Lenses) at the same frequency. Video frames were analyzed online and fluorescent signals were acquired using custom acquisition code (de Jong et al., 2019). The fluorescent signal obtained after stimulation with 405 nm light was used to correct for movement artifacts as follows: first, the 405 nm signal was fitted to the 470 nm signal using the first and second coefficients of the polynomial that was the best fit (least squares) to the 470 nm signal. The fitted 405 nm signal was then subtracted from the 470 nm signal to obtain the movement and bleaching-corrected signal. 405 nm stimulation was omitted from most dLight recordings to maximize light collection and a baseline tracking general photo-bleaching trend was subtracted instead. Although some movement may contribute to the signal detected, movement artifacts are minimized in a head-fixed setup and not expected to occlude the nicotine-related signal. Signals were normalized (Z score) based on the mean and standard deviation of signal during the pre-nicotine baseline period at 100–500 s (intact and caspase experiments) or 100–290 s (antagonist experiments) and peri-event plots for the nicotine infusions were generated. Baseline normalization was performed on the original ΔF/F signal using the time-window -2 to 0.5 sec prior to infusion. Thus, z scores accurately reflect the number of standard deviations from the mean during baseline and AUCs calculated are relative to signal immediately prior to infusion. If the AUCs of individual infusions were not normally distributed, assessed by a Kolmogorov-Smirnov test, analysis of the first infusion was performed separately from analysis of infusions 2–6.

### Behavioral assays

All behavioral tests were performed during the light phase in a temperature (68–74°F) and humidity (40–60%) controlled room that is illuminated by eight 32 W fluorescent lights each producing 2925 lumens. Behavioral equipment was cleaned with 70% EtOH and an odor remover (Nature’s Miracle) between individual animals.

### Conditioned Place Preference or Aversion (CPP or CPA)

For experiments involving IV infusions of nicotine (Figure 1), animals recovered from jugular vein catheterization for 2 days before beginning the CPP protocol. On the first pre-test day, mice were placed in the center compartment of a custom-made three-compartment chamber and allowed to explore the full chamber freely for 10 min while their movement in the chamber was recorded via a video tracking system (Biobserve). During the next 3 days, mice were placed in one side of the chamber, for 30 min, blocked from exploring the other regions, and infused with sterile, physiological 0.9% saline (volume: 1.25 μl/g) six times over 30 minutes, every five minutes, through the jugular vein catheter. In the afternoon, mice were placed in the opposite chamber for 30 min and infused with nicotine (total dose: 0.25 mg/kg or 1.25 mg/kg free base; each infusion: 41 μg/kg or 208 μg/kg) dissolved in saline every 5 minutes. Conditioning chambers were assigned according to a biased method to pair the hypothesized rewarding dose of nicotine (0.25 mg/kg) with the less-preferred side on the initial pre-test and the hypothesized aversive dose of nicotine (1.25 mg/kg) was paired with the initially preferred chamber. On the final post-test day, mice were again allowed to explore the full chamber freely for 10 min while movement was recorded. The time spent in each compartment (nicotine-conditioned, neutral, and saline-conditioned) was calculated and compared on post-test to pre-test scores to generate place preference (or avoidance) scores. For experiments involving optogenetic inhibition (Figures 6L–6P), animals recovered from fiberoptic implantation for at least 7 days before CPP. The behavioral paradigm was identical except mice were injected intraperitoneally (IP) with 10 μl/g saline immediately before the morning conditioning session and in the afternoon session, animals received 2.5 mg/kg nicotine IP (dissolved in 10 μl/g saline)

and continuous 3–5 mW 589 nm light. Nicotine reliably induces conditioned place aversion at high doses, whether delivered IP or IV. We chose to deliver aversive nicotine via intraperitoneal injection in this experiment to replicate the methods used by [Wolfman et al. \(2018\)](#) to establish the habenulo-interpeduncular axis as a regulator of nicotine aversion.

#### **Real-time place preference and aversion (Figures 5H–5J, S2H, S2I, and S6F)**

Six weeks after virus injection, mice with optogenetic implants were connected to a fiberoptic cable and placed in a custom-made three-compartment chamber (same as above). For optogenetic stimulation, the cable was connected to a 473 nm or 589 nm DPSS laser diode (LaserGlow) through an FC/PC adaptor, and laser output was controlled using a Master-8 pulse stimulator (A.M.P.I.). Power output was tested using a digital power meter (Thorlabs) and was checked before and after each experimental animal; output during light stimulation was estimated to be 3–5 mW/mm<sup>2</sup> at the targeted tissue 200 μm from the fiber tip ([www.optogenetics.org/calc](http://www.optogenetics.org/calc)). The left side of the chamber was designated as the initial stimulation side (Phase 1) and after 10 min the stimulation side was switched to the other previously non-stimulated side of the chamber (Phase 2). The middle of the chamber was a neutral area that was never paired with stimulation. At the start of each session, the mouse was placed in the middle of the chamber, and every time the mouse crossed to the stimulation side, constant laser stimulation (473 nm: 20 Hz, 5 ms pulses; 589 nm: continuous light) was delivered until the mouse exited the stimulation area. There was no interruption between Phase 1 and Phase 2. The movement of the mice was recorded via a video tracking system (Biobserve) and the time the mice spent in each area (stimulated, non-stimulated, neutral) was calculated.

#### **Open field test**

For optogenetics (Figures 5K, S2J, and S6G), mice were placed in the open field chamber and their movement was recorded and analyzed for 15 min using video-tracking (Biobserve). The 15-min session was divided into three 5-min epochs; during the first epoch, there was no light stimulation (off), during the second epoch the animal received light stimulation (on), and during the third epoch there was no light stimulation (off). Light output and frequency were the same as described in the real-time place preference section.

#### **Computational modeling**

We calculated blood-nicotine concentrations in our infusion experiment using nicotine's estimated half-life in C57BL/6J mice of 9.2 minutes ([Siu and Tyndale, 2007](#)) nicotine reaching the blood immediately upon intravenous infusion.

$$[Nic]_1 = [Nic]_0 e^{-\frac{\ln(2)}{9.2}}$$

Blood nicotine concentrations (mg/kg) were converted into brain nicotine concentrations (μM) without a multiplication factor since no empirical data was available on the relationship between blood and brain nicotine concentrations in mice and our simulated data recruited α7 receptors at the high, but not low dose of nicotine similar to observations made in mice ([Fenster et al., 1997](#); [Wooltorton et al., 2003](#)). For nicotine to reach the brain from the blood, we applied a temporal delay, given that the brain nicotine concentration peaks ~11 s after it peaks in the blood ([Berridge et al., 2010](#)); we implemented this delay by letting the brain nicotine concentration follow the blood concentration at a rate of 25% of the concentration difference per second. Then, for both the α4β2 and α7 receptors, we calculated (de)sensitization and net activation of each of the receptors based on equations modified from [Graupner et al. \(2013\)](#) with a constant baseline acetylcholine (ACh) concentration of 0.1 μM. The time course of activation and desensitization for each receptor is given by

$$\frac{dy}{dt} = \frac{(y_\infty(Nic, ACh) - y)}{\tau y(Nic, ACh)}$$

where  $\tau y(Nic, ACh)$  is the time constant where a steady state for  $y_\infty(Nic, ACh)$  is achieved. The maximal activation ( $a_\infty$ ) or sensitization ( $S_\infty$ ) for a given Nic/ACh concentration are determined by the half-maximal concentrations of nAChR activation ( $EC_{50}$ ) and sensitization ( $IC_{50}$ ) according to the following Hill equations

$$a_\infty(Nic, ACh) = \frac{(ACh + \alpha Nic)^{n_a}}{EC_{50}^{n_a} (ACh + \alpha Nic)^{n_a}}$$

$$S_\infty(Nic, ACh) = \frac{IC_{50}^{n_s}}{IC_{50}^{n_s} (Nic + \eta ACh)^{n_s}}$$

where  $\alpha$  accounts for the affinity for α4β2 ( $\alpha = 3$ ) and α7 ( $\alpha = 2$ ) receptors for Nic relative to ACh,  $\eta$  is a fraction that determines how much ACh drives receptor desensitization, and  $n_a$  and  $n_s$  represent the Hill coefficients of activation and sensitization respectively.

The time constant for receptor desensitization ( $\tau_d$ ) for a given Nic/ACh concentration is determined by the fastest time constant at which the receptor is desensitized ( $\tau_0$ ), the desensitization recovery time constant ( $\tau_{max}$ ), the concentration at which the desensitization time constant is half-minimum ( $K_r$ ), and the fraction of ACh concentration that influences the desensitization time constant ( $\eta$ ) according to the following equation:

$$\tau_d(Nic, ACh) = \tau_0 + \tau_{max} \frac{K_{\tau}^{n_{\tau}}}{K_{\tau}^{n_{\tau}} + (Nic, \eta ACh)^{n_{\tau}}}$$

Rise and decay filters were applied to each receptor activation curve to depict bulk photometry signals more accurately from the experimental data, given the relatively slow response kinetics of fluorophores (Akerboom et al., 2012) the fluorophore signal was set to follow the true receptor activation curve at a rate of 5% of the difference between the two signals per second. For the antagonist simulation (Figures 2F and 2G), sensitization was set at 20% of its baseline value (mimicking an 80% receptor desensitization by  $\alpha 4\beta 2R$  antagonist DHBE due to its fatality at high doses). For predicting the response of DA neurons (expressing  $\alpha 4\beta 2Rs$ ) that receives an  $\alpha 7$  receptor-expressing GABAergic input (Figures 4E, 4F, and 6A–6C), we subtracted the activation of an  $\alpha 7$  receptor-activated unit from the activation of an  $\alpha 4\beta 2R$ -expressing unit at 50% strength.

### Histology and microscopy

#### Immunohistochemistry and microscopy

Were performed as described previously in Lammel et al. (2012). Briefly, after intracardial perfusion with 4% paraformaldehyde in PBS, pH 7.4, the brains were post-fixed overnight and coronal brain sections (50 or 100  $\mu m$ ) were prepared. Sections were stained overnight in a primary antibody solution (rabbit anti-TH, mouse anti-TH (all Millipore), all 1:1000). Twenty-four hours later, sections were stained for 4 hours in secondary antibody solution (goat anti-mouse Alexa Fluor 488, goat anti-rabbit Alexa Fluor 488 (all Thermo Fisher Scientific), all 1:750). Image acquisition was performed with Zeiss LSM 710 laser scanning confocal microscope using 20x or 40x objectives and on a Zeiss AxioImager M2 upright widefield fluorescence/differential interference contrast microscope with charge-coupled device camera using 5x, 10x and 20x objectives. Images were analyzed using ImageJ. Sections were labeled relative to bregma using landmarks and neuroanatomical nomenclature as described in “*The Mouse Brain in Stereotaxic Coordinates*” (Franklin and Paxinos, 2013). All images presented with multiple colors represent a composite of images collected with different excitation wavelengths.

#### In situ hybridization

To determine the extent of co-expression of VGLUT2 and GAD2 in LDT neurons (Figure S4A), we combined Cre-dependent viral fluorophore expression with *in situ* hybridization. Probe sequence for the *Vglut2* and *Gad1* and *Gad2* DIG RNA probes as well as the free floating *in situ* protocol were adapted from Weissbord et al. (2014). GAD2-Cre (n = 2 mice) and VGLUT2-Cre (n = 2 mice) mice were injected with 500 nl AAV5-EF1 $\alpha$ -DIO-eYFP into the LDT. Two weeks later, the animals were euthanized and 100  $\mu m$  sections of the LDT were sliced and washed in diethyl pyrocarbonate (DEPC)-treated PBS and treated with a 7  $\mu g/ml$  proteinase K solution for 10 min at 37°C. Proteinase K was inactivated using 4% PFA in PBS, which was followed by washing in PBS and acetylation in 0.25% acetic anhydride in 0.1 M triethanolamine in DEPC-treated water. Tissue sections were incubated overnight in hybridization solution (50% deionized formamide, 1x Denhardt’s, 10% Dextran sulphate and 5x Saline-Sodium Citrate (SSC) with 100 ng/ml probe at 55°C. Stringency washes were in 2x SSC with 50% formamide for 1 hour, and in 2x SSC and 0.2x SSC for 20 min, each at 65°C. This was followed by blocking for 1 hour in DIG blocking buffer (Roche) and overnight incubation at 25°C in 1:1000 Anti-Digoxigenin-AP FAB fragments (Roche). Slices from the VGLUT2-Cre animals were incubated with probes for *Gad1/2* RNA and slices from GAD2-Cre animals were incubated with probes for *Vglut2* mRNA. Because the *in situ* hybridization procedure attenuates fluorescence, tissue sections were co-stained with a chicken anti-GFP (1:1000, Abcam). Primary antibody incubation was for 2 hours and was followed by washing steps in DIG wash buffer (Roche) and incubation with secondary antibodies (Alexa Fluor 546 goat anti-rabbit, Alexa Fluor 647 goat anti-mouse (all 1:750, Thermo Fisher Scientific) and Alexa Fluor 477 goat anti-chicken (1:750, Abcam) as well as the alkaline phosphatase substrate reacting with NBT/BCIP in detection buffer (Roche). Slides were imaged on a Zeiss AxioImager M2 microscope using a 20x objective. Quantification of co-expression was manually counted using ImageJ.

#### Whole brain input mapping

To map inputs to LDT<sub>GABA</sub> → VTA and LDT<sub>Glutamate</sub> → VTA neurons (Figures S4E–S4I), we used a rabies virus-based genetic mapping strategy to label presynaptic inputs onto designated starter cell populations, and quantified input cell data using a customized, semi-automated whole-brain mapping Matlab script. Specifically, VGLUT2-Cre (n = 4 mice) and GAD2-Cre (n = 3 mice) mice were injected with AAV-FLEX-TVA-mCherry (i.e., a cellular receptor for subgroup A avian leukosis viruses) and AAV-FLEX-RG (i.e., rabies virus glycoprotein; 250 nl, 1:1) into the LDT and four weeks later, 300 nl RV-EnvA-ΔG-GFP (i.e., pseudotyped, glycoprotein-deficient, GFP-expressing rabies virus) was injected into the VTA (see “*Stereotaxic Injections*” for coordinates). Seven days after injection, mice were perfused with 4% PFA in PBS. For input mapping, 50  $\mu m$  sections of the whole brain, excluding the olfactory bulb and cerebellum, were prepared, and scanned using a Zeiss Axio Scan Z1 microscope. Individual slices were aligned using customized Matlab scripts. GFP-positive pixels were identified on the basis of a pixel-intensity threshold in the green channel. False-positive pixels (artifacts) were manually identified and removed. Positive pixels were assigned to different brain areas based on “*The Mouse Brain in Stereotaxic Coordinates*” (Franklin and Paxinos, 2013). Pixels per brain area were then represented as a percentage of total input pixels. 31 slices were randomly selected to validate this semi-automated quantification method and a human observer counted GFP-positive cells in these regions. These results demonstrated a high correlation between manual scoring of input neurons by an independent observer and our automated segmentation procedure ( $R^2 = 0.9$ , n = 31 slices).

### **Fluorescent *in situ* hybridization**

The fluorescent *in situ* hybridization experiments (Figures S4J and S4K) were conducted using a commercially available RNAscope® Multiplex Fluorescent Reagent Kit V2 (ACD Bio, USA). Brains were extracted and snapfrozen by submerging them into frozen isopentane (-70 to -50°C). They were stored in an airtight container in a -80°C freezer. 16 µm coronal LDT brain slices were prepared using a cryostat, placed on Superfrost Plus microscope slides (Fisher Scientific, USA) and stored in a -80°C freezer. On the next day, brain slices were fixed in 4% paraformaldehyde (PFA) in PBS (30 min) followed by an ethanol dehydration procedure (20 min). Slices were then bathed in hydrogen peroxide (10 min), followed by protease IV from the RNAscope® kit (15 min). Next, probe mixes were made containing  $\alpha$ 7R (Mm-Chrna7), GAD2 (Mm-Gad2). Probe mixes were applied to the brain slices for hybridization (2 hours at 40°C). After amplification of the signal (using AMP1, AMP2 and AMP3 from the RNAscope® kit), channel C1 was developed using green Opal 520 (Akoya Biosciences, USA) and channel C2 was developed using orange Opal 570 (Akoya Biosciences, USA). Lastly, nuclei were stained using DAPI (from the RNAscope® kit) and brain slices were sealed with ProLong Gold Antifade mountant (Thermo Fisher Scientific, USA) and a glass coverslip. Images were taken using a confocal microscope (LSM710, Carl Zeiss Inc.) at 5 different z depths (spanning 4.4 µm), and images were flattened by taking the maximum projection across the z direction. Regions of interest (ROIs) were identified using a machine learning-based segmentation algorithm NucleAlzer37 based on the DAPI channel. The amount of visible mRNA across the DAPI-identified region was used as a proxy for total mRNA in the cell. All identified regions of interest were manually sorted by an investigator who was blind to brain region and probe mix. ROIs were removed if they (i) showed overlap with other regions of interest or (ii) were segmentated inadequately by the algorithm. Using a custom-made MATLAB algorithm, the remaining cells were analyzed based on the percentage of DAPI-positive pixels that were also positive for targeted mRNA. To adjust for potential differences in staining and/or image quality, we compared pixels in all regions of interest to background fluorescence levels in each image. To do this, we first established a 'null distribution' that quantifies the distribution in pixel intensity values for cells putatively negative for targeted mRNA. Each cell's distribution of pixel intensities was compared to the null distribution for the targeted mRNA and a correlation coefficient R was calculated. If R of a cell's distribution compared to the null distribution was less than 0.85, then a cell was labeled as positive for the targeted mRNA.

### **QUANTIFICATION AND STATISTICAL ANALYSIS**

Student's t tests (paired and unpaired), one-way or two-way ANOVA tests, and mixed effects analyses were used to determine statistical differences using GraphPad Prism 9 (Graphpad Software). Kolmogorov-Smirnov tests were performed on AUCs of individual infusions to check for a normal distribution. Holm-Sidak's post hoc analysis was applied when a one-way ANOVA or mixed effects analysis showed a significant main effect, or a two-way ANOVA or mixed effects analysis showed a significant interaction. Statistical significance was \*  $p < 0.05$ , \*\*  $p < 0.01$ , \*\*\*  $p < 0.001$ . All data are presented as means  $\pm$  SEM. All details of the statistical analysis including means, SEMs, and number of animals used are summarized in Table S1.